Computers and Geotechnics 85 (2017) 230–248

Contents lists available at ScienceDirect

Computers and Geotechnics

journal homepage: www.elsevier.com/locate/compgeo

Research Paper

Monitoring and numerical analysis of behaviour of Miaojiaba concrete-face rockfill dam built on river gravel foundation in China

Lifeng Wen [a], Junrui Chai [a,b,*], Zengguang Xu [a], Yuan Qin [a], Yanlong Li [a,*]

[a] State Key Laboratory Base of Eco-hydraulic Engineering in Arid Area, Xi'an University of Technology, Xi'an 710048, PR China
[b] College of Hydraulic and Environmental Engineering, China Three Gorges University, Yichang 443002, PR China

ARTICLE INFO

Article history:
Received 20 June 2016
Received in revised form 23 November 2016
Accepted 19 December 2016
Available online 9 January 2017

Keywords:
Concrete face rockfill dam
Deformation behaviour
River gravel foundation
Monitoring
Numerical analysis

ABSTRACT

This study evaluated the behaviour of a concrete face rockfill dam (CFRD) built on river gravel foundation on the basis of in-situ measurement records and numerical analysis. The monitoring records were obtained from a detailed deformation-monitoring system. A 3D finite element analysis was performed to assess long-term dam behaviour. The behaviour of the CFRD built on river gravel foundation was analysed comprehensively. A discussion of behaviour, especially with relevance to the behaviour of dams built on stiff-foundation, was included. The effect of the river gravel foundation was analysed, and the exact mechanisms were discussed. The relative contribution of various factors on the long-term behaviour of the CFRD was also studied. In-situ measurements were compared with numerical results to discuss the capability of the numerical model to predict the dam behaviour.

1. Introduction

Concrete face rockfill dams (CFRDs) are commonly constructed worldwide because of their short construction period, cost effectiveness and excellent resistance to post-construction deformation and leakage [1,2]. An increasing number of CFRDs are being built on deep river gravel foundations because of their adaptability to geology. Examples of such dams include the 122 m-high Reece Dam in Australia, which was completed in 1986 [3], and the 136 m-high Jiudianxia Dam in China, which was completed in 2008 [4]. Alluvium is widely distributed in most rivers in Western China, particularly in the southwestern region. This type of soil is characterised by looseness, lithological discontinuance and poor particle size distribution [5]. Alluvium is mainly composed of gravel, crushed rocks and fine sand, with a general porosity ratio of 0.21–0.33, a dry density of 2.0–2.3 g/cm^3 and a friction angle of 33–46° [5]. Alluvium may cause geological problems in actual engineering, such as compressive deformation, differential settlement, leakage and seepage deformation, foundation liquefaction and shear failure [6].

A number of case studies related to the construction of embankments or dams on soft clay foundations have been conducted, considering that large deformations and long-term consolidation on the foundation soil could threaten the safety of these structures [7–15]. The effect of river gravel foundation, which has stronger permeability and a larger grain size than clay foundation, on dam behaviour has yet to be fully considered, although many dams have been built on it. Wang et al. [16] adopted a coupled hydro-mechanical (HM) method to assess the performance of the foundation treatments of a dam built on an alluvium foundation, but they only concentrated on the performance of the foundation. Wang and Liu [6] and Wang et al. [17] analysed the behaviour of a rockfill dam built on depth soft alluvial deposit based on finite element analysis (FEA). However, their numerical model was simple and failed to obtain the deformation mechanism of the foundation. Studies on the behaviour of CFRDs built on river gravels remain limited. Gan et al. [4] predicted the long-term behaviour of a CFRD built on sand and gravel foundation considering the creep effect, but their model could not capture other aspects of material behaviour, such as seepage and partly saturated soil behaviour. Xu et al. [18] adopted centrifugal tests to study the CFRD behaviour. Although the results provided useful insights, they were limited. Wen et al. [19] analysed the CFRD behaviour on sand and gravel foundation, but they did not consider the time effect. The behaviour of CFRDs built on river gravel foundation is still not well-understood. Extensive studies are necessary to understand dam behaviour and thus fully utilise river gravels as dam foundation.

This paper presents a combined study of in-situ measurement records and numerical analysis of the behaviour of a CFRD built on river gravel foundation. The monitoring records covered the stages of dam construction, initial reservoir filling and first year

* Corresponding authors at: NO. 5 South Jinhua Road, Xi'an, PR China.
E-mail addresses: jrchai@xaut.edu.cn (J. Chai), lylong2356@126.com (Y. Li).

http://dx.doi.org/10.1016/j.compgeo.2016.12.018
0266-352X/

Nomenclature

p	average stress
q	principal shear stress
E_t	tangent modulus
R_f	failure ratio
μ_t	tangential bulk modulus
φ	friction angle
φ_0, $\Delta\varphi$	two constants related to friction angle
σ_1, σ_3	major and minor principal stresses
S	stress level
K	modulus number
G, F, D	model parameters
P_a	atmospheric pressure
m	modulus exponent
$\varepsilon_L(t)$, ε_L	axial creep strain
t, Δt	time and increment time for creep model
c_L, d, η, m_L	axial creep parameter
$\varepsilon_V(t)$, ε_V	volume strain
ε_{Vf}	volume creep strain limit
λ_V	volume creep strain rate coefficients
α_V, β_V	volume creep coefficient
c_α, d_α, c_β, d_β	volume creep parameter
ε_{Lf}	axial creep strain limit
λ_L	axial creep strain rate coefficients
$\mathbf{D}$	tangential elastic modulus tensor
u	displacement vector
α	Biot's coefficient
p_w	pore water pressure
δ	Kronecker delta tensor
f	body force tensor
$H(\phi\text{-}z)$	heaviside function
ρ_w	density of water
S_w	specific storage
ϕ	total water head
v	flow velocity
k, k_0	current and initial hydraulic conductivity
n, n_0	current and initial porosity
x_i	parameter to be inverted
s	number of monitoring points
k_1	number of time points
$\mathbf{P}(j)$	initial population
j	number of current generation
p_1	individual number

of operation. The numerical analysis was conducted by FEA, in which the mechanical behaviour of river gravel and rockfill was represented by an elasto-plasticity model and a creep model, respectively. A coupled HM analysis method was adopted to simulate the HM coupling process. The input parameters were obtained via a back analysis method based on genetic algorithms. In-situ measurements were compared with the numerical results and data on stiff-foundation dams. The effect of river gravel foundation on the CFRD behaviour was analysed, and the exact mechanisms were discussed. The effect of various factors on the dam behaviour was analysed. The capability of the numerical model to predict the dam behaviour was also discussed.

2. Miaojiaba CFRD

2.1. General

The Miaojiaba Project is located in Bailongjiang River, Wenxian City, Gansu Province, China. This project aims to provide energy with an annual output of 9.24 billion kW h. The total storage capacity of the dam is 2.68 billion m^3, and the normal water level is 800 m. A CFRD functions as the water-retaining structure. The layout and typical section of the dam are shown in Fig. 1. The dam height is 111 m, with a crest of 348.20 m in length and 10.0 m in width. The rockfill volume of the dam body is approximately 3.77 million m^3. A slot-type, concrete cutoff wall is designed to control foundation seepage. The thickness and maximum depth are 1.2 m and 50 m, respectively. The face slab is composed of C25 concrete, with axial compressive and tensile strengths of 16.7 MPa and 1.78 MPa, respectively. The thickness is 0.3 m at a top elevation (EL) of 805 m and 0.618 m at a bottom EL of 700 m. The toe slab and connecting plate are founded above river gravels.

2.2. Site condition and compaction effort

As shown in Fig. 1c, the dam site has 44–50 m-thick deep alluvium (river gravel), which can be classified into the following four groups from bottom to top: 5–10 m-thick sand and gravel with block gravel layers (Q_4^{a1}), 12–15 m-thick gravel layer (Q_4^{a2}), 6–20 m-thick sand and gravel with gravel layers (Q_4^{a3}) and 2–4 m-thick reservoir alluvium layer. The bedrock below alluvium is composed of metamorphism tuff. No strong weathering zone is distributed in the bedrock.

The reservoir alluvium layer was excavated, and compaction effort was exerted to handle the remaining loose surface layer. Field compaction tests were performed to determine the construction parameters. A 2.2 m towed vibrating roller with mass of 25,000 kg was used. Two sites were selected at the downstream and right side of the river. Each site contained two compaction zones with pass numbers of 8 and 10. Fig. 2 shows the particle size distribution before and after compaction. The particle breakdown increased the percentage of small particles (<5 mm) from 16.06% to 20.74%, and the largest particle size decreased from 600 mm to 500 mm. The average values of the field compaction test results are shown in Table 1. River gravels were compacted to a high density because of the breakdown and structure adjustment of particles. Compared with the original dry density, the density was increased by 12% after field compaction. The densities at the two test sites were both greater than 2.10 g/cm^3 (i.e. the designed value). The particles became finer and the relative density became higher as the rolling pass number increased. A pass number of 10 was recommended for field compaction.

Sampling and dynamic penetration tests were conducted to evaluate the effectiveness of the compaction effort. Compaction effectiveness decreased with depth. Foundation improvement was mainly limited to a surficial layer with a depth of 6 m based on the dynamic penetration test results. The improvement effect on the 4 m surficial layer was evident. The dry and relative densities, bearing capacity and compressive modulus increased, whereas the permeability and porosity decreased significantly. The dry density and bearing capacity increased slightly within the range of 4–6 m below the surface. At a depth of 6 m, the average bearing capacity was 586 kPa before compaction and 610 kPa after compaction. For the foundation that exceeded 6 m below the surface, no significant improvement was observed after field

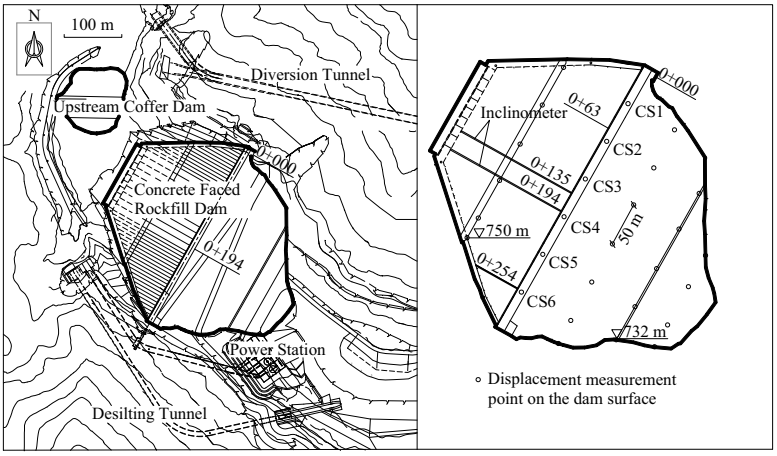

(a) Layout of Miaojiaba CFRD and arrangement of displacement measurement points on dam surface

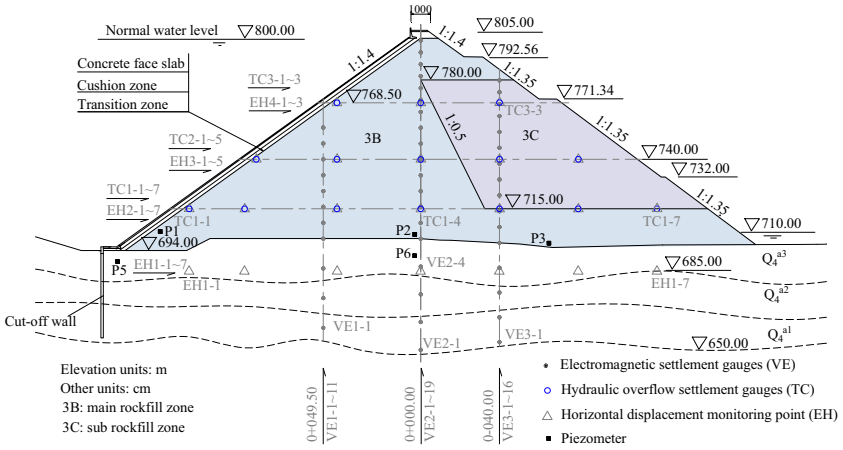

(b) Typical cross section of the Miaojiaba CFRD and location of instrumentation equipment

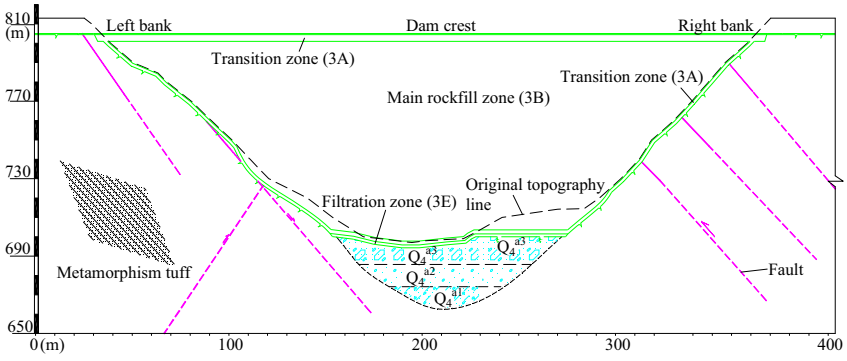

(c) Longitudinal section of Miaojiaba CFRD along dam axis

Fig. 1. Layout and typical section of Miaojiaba CFRD.

compaction. However, its average in situ density was 2.15 g/cm^3, which was greater than the designed value.

Table 2 shows the physical and mechanical properties of the river gravel layers after compaction has been achieved from a series of field and laboratory tests. Gradation analysis showed that the percentage of coarse particles (5–500 mm) was over 80%, that of small particles (<0.075 mm) was less than 5% and that of clay content was less than 3%. The river gravels were typical coarse granular materials. They were free draining and had average hydraulic conductivity of 1.6×10^{-4} m/s.

2.3. Construction materials and scheme

The dam zoning is shown in Fig. 1b. The cushion material was composed of artificially blended sand and gravel. The rockfill and transition materials were from the quarry. The mineral content

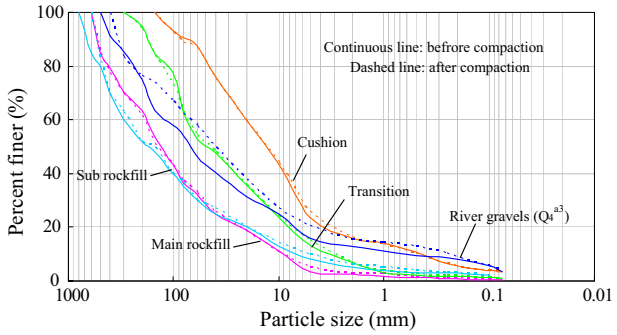

Fig. 2. Gradation curve of river gravels and dam construction materials.

was mainly thick massive metamorphic tuff with a dry density of 2.70–2.72 g/cm^3, porosity of 0.51–0.80% and saturated compressive strength of 102–131 MPa. The main rockfill (3B) and sub rockfill (3C) materials were from the same origin and had the same mineralogy with compressive strength of 120 MPa. However, these materials had different particle size distributions; the maximum particle size for both materials was 800 mm. A series of compaction tests was also conducted for the dam materials. Fig. 2 shows that the particle gradation changes of the dam construction materials (rockfill, transition and cushion) were insignificant before and after compaction. The compacted main rockfill and sub rockfill materials had dry densities of 2.35 g/cm^3 and 2.25 g/cm^3 and void ratios of 0.19 and 0.20, respectively. The oedometer tests indicated that the rockfill materials had low compressibility, with the main and sub rockfill materials having compression moduli of 128 MPa and 97 MPa, respectively. The main and sub rockfill materials adopted the same construction parameters and methods. The details of the dam materials and field compaction methods are presented in Fig. 3.

The dam construction was divided into four stages. The construction of the cutoff wall began in September 2009 and was completed in October 2009. The dam construction commenced in October 2009 and was completed in November 2010 for the dam body and in February 2011 for the face slab. The reservoir filling process started in May 2011, and the water level reached an EL of 800 m in July 2011.

2.4. Deformation-monitoring system

A detailed monitoring system was used because of the technical characteristics of the dam combined with the adverse site conditions. The details of the monitoring instruments installed in the Miaojiaba Dam are listed in Table 3. The monitoring system measured the deformations, stresses and strains in the dam and other impervious structures, as well as the pore water pressure in the dam and foundation.

3. Monitoring result analysis

3.1. Crest settlement measurements

The available time series for the dam crest measurement points (CS1–CS6) was from November 2010 to April 2012. This time series covered the post-construction stage, reservoir filling stage and 8 months of operation time. Fig. 4a shows the settlements as functions of time, and Fig. 4b shows the distribution of settlements along the crest axis. The maximum rate considerably decreased from 13.0 mm per month in July 2011 to 3.5 mm per month in November 2011. The settlement rate increased when the reservoir level rose rapidly from 710 m to 800 m, which could mainly be caused by the water pressure and wetting deformation as a result of the reduction in rockfill particle strength induced by wetting. The settlement growth rate increased several days after the reservoir level had risen. This phenomenon was attributed to the gradual increase in water pressure and the water infiltration rate being slower than the reservoir level-rising speed. The settlement in the middle was larger than that near tail ends because of the differences in the height of the measurement points. The maximum settlement was 279 mm (0.25H%, H: dam height) in CS4 at 8 months after reservoir filling.

Fell et al. [22] reported that crest settlements that occurred shortly after the first reservoir filling generally ranged from 0.02H% to 0.05H% and from 0.10H% to 0.15H% for rockfill with high- and intermediate-strength mineralogy, respectively. By contrast, long-term (over 10 years) crest settlements generally ranged from 0.10H% to 0.2H% and from 0.10H% to 0.3H% [20]. Clements [23] proposed that long-term crest settlement for a modern compacted CFRD was approximately 0–0.25H% in general. Sherard and Cooke [24] obtained the range of 0.1–0.25H%. The crest settlement of the Mioajiaba CFRD was closest to the maximum value of these case histories. The large settlements that occurred shortly after reservoir filling were related to dam height, rockfill and foundation properties (i.e. low-strength mineralogy, crushable particles and poor particle size distribution) and construction technique. The river gravel foundation might be the main reason for the large settlement. Most of the case histories presented earlier involved construction on an intact rock foundation.

Crest settlement behaviour comprises two main components, namely, time-dependent deformation and the deformation caused by the initial reservoir filling. Approximately 10–40% of the total crest settlement of a stiff-foundation dam is caused by reservoir filling [20], and 85% occurs during the first year after the commencement of reservoir filling [21]. For the Miaojiaba CFRD, 70% of the crest settlement occurred before the first reservoir filling was completed. Such settlement was larger than that in a stiff-foundation dam and was due to two reasons. Firstly, the dam behaviour was dependent on the inherent heterogeneity of particle size distributions and void ratios. Consequently, poorly graded particle size distribution and inadequate compaction during construction might result in a large deformation during the reservoir filling period. Secondly, the river gravel foundation generated significant deformation before the completion of the first reservoir filling, thereby causing a large crest settlement. These results indicated that water load was an important factor in dam crest settlement.

3.2. Internal settlement measurements

Fig. 5 shows the progression of vertical displacements observed at seven HSG monitoring points at an EL of 715 m in cross section 0 + 194. The curves indicated that the settlement accumulated over

Table 1
Results of field compaction tests of river gravels.

Test site	Compaction zone	Dry density (g/cm^3)	Relative density	Porosity (%)	Settlement (cm)
Dam downstream 95 m, right side of the river	8 passes	2.16	0.84	20.1	16.88
	10 passes	2.21	0.92	19.2	17.09
Dam downstream 7 m, right side of the river	8 passes	2.14	0.81	20.5	17.23
	10 passes	2.22	0.93	19.7	17.57

Table 2
Average values of the physical and mechanical properties of river gravel layers.

River gravels	Thickness (m)	Materials	Clay content (%)	Dry density (g/cm^3)	Relative density	Hydraulic conductivity (m/s)	Deformation modulus (MPa)
Q_4^{a1}	5–10	Sand and gravel, block gravel	<3	2.20	0.85	1.7×10^{-4}	35
Q_4^{a2}	12–15	Gravel	<3	2.15	0.82	1.7×10^{-4}	50
Q_4^{a3}	6–20	Sand and gravel, gravel	<3	2.20	0.91	1.4×10^{-4}	40

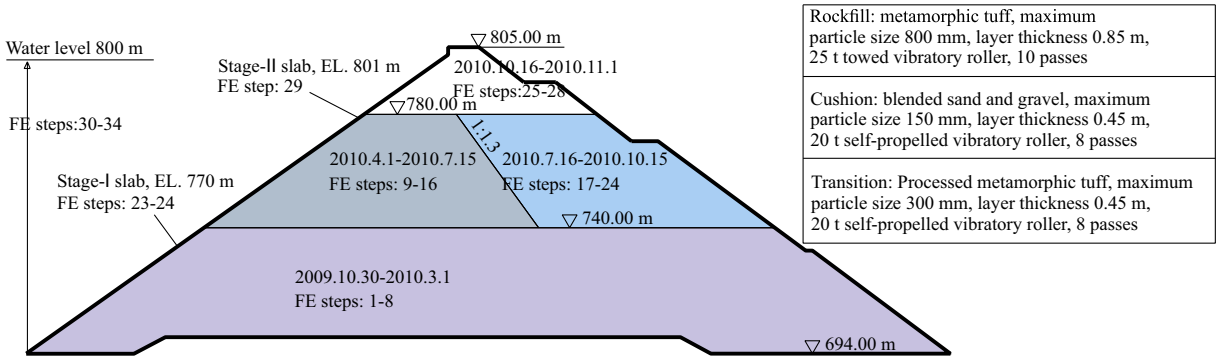

Fig. 3. Construction process and details of Miaojiaba CFRD.

Table 3
Monitoring system installed in Miaojiaba Dam.

Instrumentation	Measuring object	Description
Survey points	Settlement at crest and on surface	13 reference stations, 5 monitoring lines (28 monitoring points), shown as Fig. 1a
Electromagnetic settlement gauges (ESGs)	Internal settlement	3 monitoring lines in section 0 + 194, shown as Fig. 1b
Hydraulic overflow settlement gauges (HSGs)	Internal settlement	7 monitoring lines (25 monitoring points) in four sections, three in 0 + 194, shown as Fig. 1b
Displacement transducers	Horizontal displacement	22 monitoring points in section 0 + 194, shown as Fig. 1b
Earth pressure cells	Stress	12 monitoring points (EC1–12) in section 0 + 199
Fixed inclinometers	Face slab movement	3 groups in face slab (shown as Fig. 1a), 2 groups in cutoff wall
Strainmeters	Strain	19 groups in face slab, 10 groups in cutoff wall
Piezometers	Pore water pressure	4 monitoring points (P1-4) in section 0 + 194, 3 monitoring points (P5-7) in river gravel foundation, shown as Fig. 1b

time. Dam deformation was mainly caused by the weight load of the rockfill, water pressure and creep deformation. During construction, settlement rapidly increased with a continuous increase in weight load. Over 80% of the total settlement occurred after dam construction. During reservoir filling, settlement increased with water pressure, but the rate was slower than that during dam construction. A high settlement increment was observed near the upstream shell under water pressure.

The measured maximum accumulated settlements at EoC and 1 year after reservoir filling were 806 mm (0.73H%) and 910 mm (0.83H%) near the dam base (EL of 725 m), respectively. In general, the accumulated settlement of a CFRD should not exceed 1.0H%. For stiff-foundation dams with a height below 150 m, the settlements should always be less than 1.0H% [25]. Jiang and Cao [26] reported that long-term accumulated settlement ranged from 0.15H% to 0.45H%, which occurred at the mid-height of a dam, based on the monitoring results of in-service stiff-foundation dams in China. Other investigators have also asserted that maximum settlement occurs at mid-height [1,2,27,28]. In the current study, the location of the maximum settlement was clearly close to the dam base, and the value was larger than those in most case histories but remained within the suggested range. The large foundation deformation was the main factor that contributed to the large dam settlement.

3.3. Horizontal displacement measurements

The observed horizontal displacements in cross-section 0 + 194 during dam construction and reservoir filling are shown in Fig. 6.

Outward displacements were observed in the upstream and downstream faces at EoC. The horizontal displacements were nearly symmetrical along the dam axis after construction because the valley was considerably symmetrical. The horizontal displacement gradually increased as it approached the upstream and downstream sides, which was similar to that of a stiff-foundation dam [27,29]. The maximum horizontal displacement occurred in the foundation and was significantly less than the settlements (EL of 685 m). The maximum value occurred at a height of 0.45 H from the dam bottom for a stiff-foundation dam [27,29], which indicated that the maximum value location moved downward under the effect of the foundation. The maximum horizontal displacements after construction were 16.7 cm (0.15H%) and 20.1 cm (0.18H%) on the upstream and downstream sides, respectively. Water pressure pushed the dam downstream. The maximum incremental horizontal displacement of 25.0 cm (0.23H%) occurred near the dam base (EL of 730 m) of the upstream face. The displacements diminished towards the downstream face.

3.4. Movement of face slab and cutoff wall

Fig. 7 shows the progression of the maximum deflection of the face slab and the displacement of the cutoff wall with time. Water pressure caused a rapid deformation rate in the face slab. The maximum incremental deflection was 15 cm (approximately 60% of the total deflection) after reservoir filling as a result of the face slab both settling and moving horizontally downstream. This result

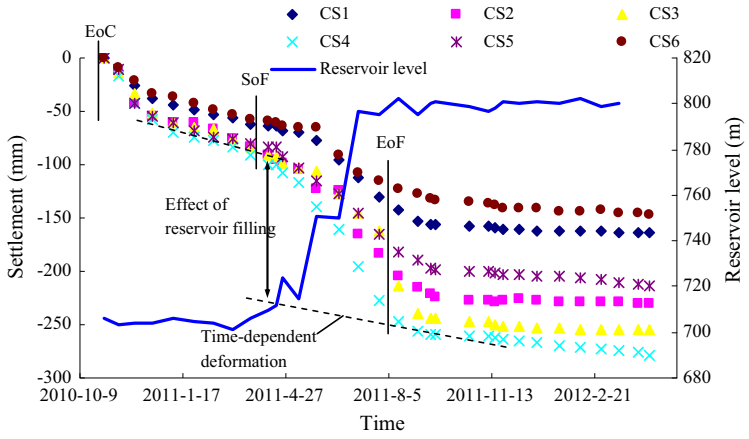

(a) Settlement of six measurement points as functions of time. EoC, end of construction; SoF, start of reservoir filling; EoF, end of reservoir filling

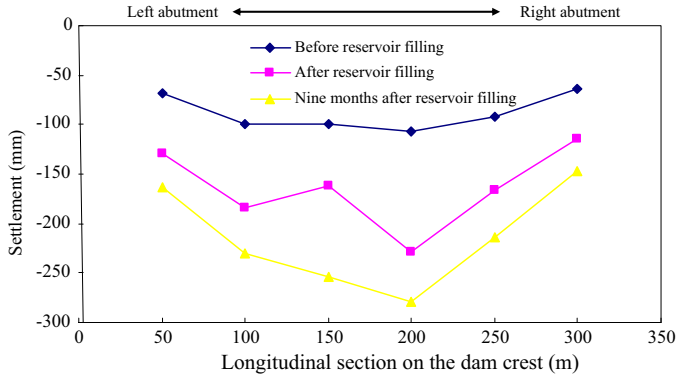

(b) Distribution of settlement along crest axis at different stages

Fig. 4. Settlement measurements on dam crest from November 2010 to April 2012.

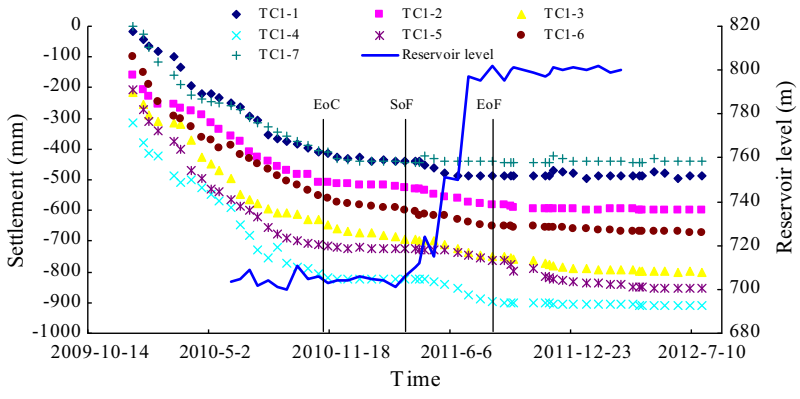

Fig. 5. Internal settlement measurements at an EL of 715 m in cross section 0 + 194.

indicated that face slab deflection was significantly affected by water load. Won and Kim [20] reported that approximately 80% of the total long-term face slab deflection of stiff-foundation dams occurred during the first reservoir filling. Fitzpatrick et al. [28] reported that the average deformation rate was approximately 3 mm per year during the first 10 years after reservoir filling. In the current study, the average deformation rate decreased to 1 mm per month after reservoir filling, and this value was higher than that for stiff-foundation dams. This result might be attributed to the large post-construction deformation of the foundation and the underlying rockfill. The largest deflection was 300 mm (0.27H %), which occurred near the dam base (EL of 728 m) 1 year after reservoir filling.

Seo et al. [30] reported that the face slab deflections in the 25 in-service dams they examined were less than 0.3H%. The long-term deflection of a stiff-foundation dam was reported to generally range from 0H% to 0.2H% [20], whereas the maximum deflection occurred in the middle [31–33] or one-third of the dam height

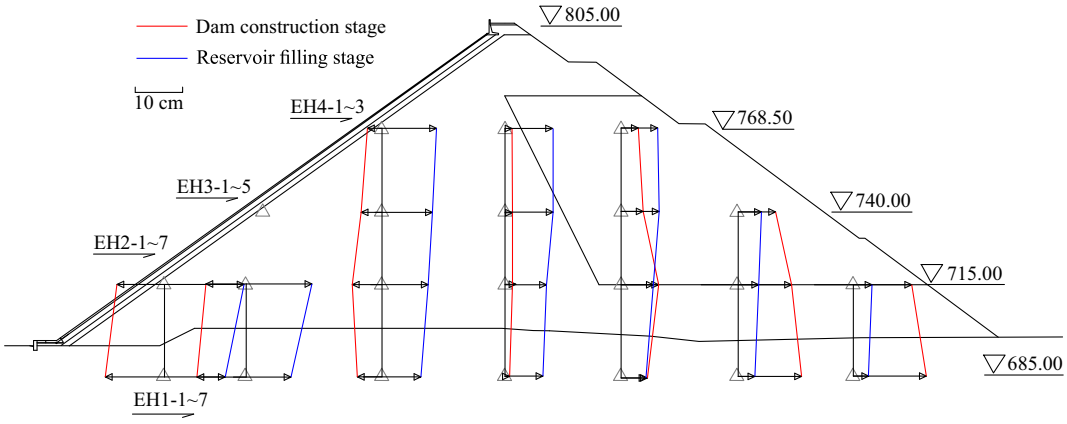

Fig. 6. Observed horizontal displacements after construction and reservoir filling in cross-section 0 + 194.

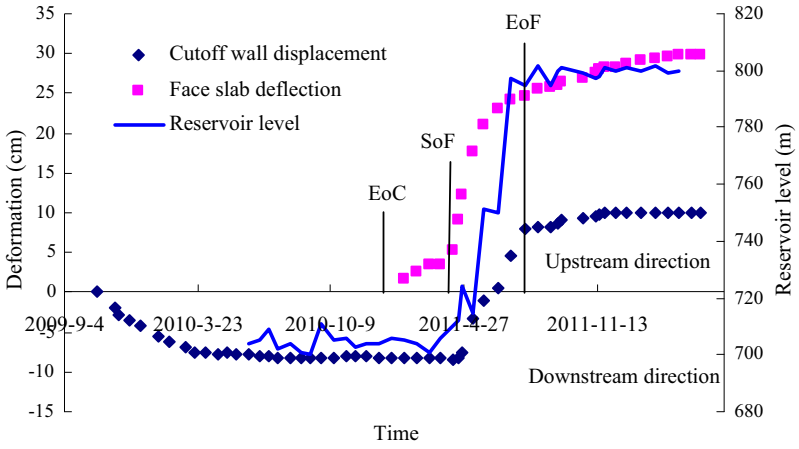

Fig. 7. Observed maximum face slab deflection and cutoff wall displacement.

[34]. The Miaojiaba CFRD had a large deflection located close to the dam base. These results could be attributed to the same factors that led to the large dam settlement.

The cutoff wall displacements were in the upstream direction before reservoir filling. The displacement shifted towards the opposite direction under the effect of water load after reservoir filling. During construction, displacement occurred mainly in the first 4 months. Approximately 90% of the deformation occurred during this stage.

4. Numerical analysis of behaviour of Miaojiaba Dam

4.1. Stress–strain relation for river gravels and rockfills

FEA was conducted to understand the dam behaviour and its mechanisms further. Large-scale unidimensional and triaxial tests were conducted to investigate the behaviour of river gravel used as the foundation for the Miaojiaba CFRD. The test results showed that the gravel compressibility decreased with increasing normal stress. The drained triaxial test results indicated that the deviatoric stress and axial strain relationship curve increased with increasing confining pressure. If the confining pressure was small (e.g. 0.1 MPa), the gravel dilated significantly after minimal compression, whereas a continuous contraction could be observed if the confining pressure was large. The volumetric strain changed from dilation to contraction with increasing confining pressure. According to the test results, the shear strength of gravelly soil could be formulated using Mohr–Coulomb failure criterion.

The capability of numerical analysis to predict the behaviour of earth and rockfill materials largely relies on the availability of a reliable constitutive model. A large number of constitutive models based on either theoretical assumptions or test observations have been proposed to simulate the behaviour of different soil types [1,8,10,19,27,29]. The behaviour of coarse granular materials, such as gravelly soil and rockfill material, which have a larger grain size than sand, has yet to be specifically considered. The nonlinear elasticity Duncan–Chang E-B model is one of the most widely used models for gravelly soil because of its ability to describe the nonlinear behaviour compared with in situ measurement results of in-service CFRDs [4,19,32,33] and determination of parameters. However, the E-B model does not consider the dilatancy and plastic deformation. A two-yield surface elasto-plasticity model for gravelly soil [35] was used in this study to describe the behaviour of river gravel foundation and rockfill materials. The model has been successfully used to simulate the construction of several CFRDs [35–38]. The main feature of the model is its ability to capture volumetric strain behaviour, including dilation, contraction and change from dilation to contraction with increasing confining pressure.

The following assumption on the two yield surfaces was used, where p is the average stress, and q is the principal shear stress:

$$\begin{cases} f_1 = p^2 + 4q^2 \\ f_2 = \frac{q^2}{p} \end{cases} . \tag{1}$$

The two yield surfaces were used to judge whether plastic strain occurred. According to a yield surface, a partial plastic strain

was introduced to describe the plastic strain. If $f_1 > (f_1)_{max}$ or $f_2 > (f_2)_{max}$, a partial plastic strain occurred, where f_1 and f_2 are the current values of yield surface functions, and $(f_1)_{max}$ and $(f_2)_{max}$ are the maximum historical values. The associated flow rule was adopted to determine the plastic strain direction. The plasticity coefficients A_1 and A_2 were introduced to describe the elasto-plasticity modulus matrix corresponding to a yield surface. A_1 and A_2 were derived using the tangential slopes of the deviation principal stress–axial strain relationship and volumetric-axial strain relationship under triaxial test conditions, E_t and μ_t. The tangential modulus E_t can be expressed as follows:

$$E_t = KP_a\left(\frac{\sigma_3}{P_a}\right)^m (1 - R_f S)^2, \tag{2}$$

where R_f is the failure ratio, σ_3 is the minor principal stress, K is the modulus number, P_a is the atmospheric pressure, and m is the exponent that defines the effect of confining pressure on the initial modulus. $S = (\sigma_1 - \sigma_3)(1 - \sin\varphi)/2\sigma_3\sin\varphi$ was defined as the stress level. Friction angle φ changed with confining stress, where φ_0 and $\Delta\varphi$ are two constants.

$$\varphi = \varphi_0 - \Delta\varphi \cdot \log(\sigma_3/P_a). \tag{3}$$

A new simple formulation of tangential bulk modulus μ_t was proposed on the basis of the test results to describe the volumetric behaviour, where G, F and D are model parameters, and σ_1 is the major principal stress.

$$\mu_t = 1 - 2\left(G - F\log\left(\frac{\sigma_3}{P_a}\right) + \frac{D(\sigma_1 - \sigma_3)(1 - R_f S_1)}{E_t}\right). \tag{4}$$

The elasto-plasticity model had eight parameters, i.e. φ, $\Delta\varphi$, R_f, K, m, G, F and D, which could be evaluated using triaxial tests. The values of the parameters of the dam construction materials and river gravel obtained from the triaxial test results are presented in Table 4. A comparison of the model predictions of the stress–strain relationship of the river gravels with the triaxial test results is provided in Fig. 8. The predicted curve showed good agreement with the test results, which indicated that the model could capture the main behaviour of the river gravel. The E-B model was also used to predict the dam deformation to analyse the potential effect of dilatancy and plastic deformation.

4.2. Creep model for river gravels and rockfills

Although coarse granular materials, such as rockfill and river gravel, are not typically expected to show time-dependent behaviour, appreciable time-dependent movements have been observed at rockfill dams, even though no changes occur in the loading [4,33,39]. The long-term settlement (creep) is mainly caused by delayed grain fracture processes [40,41]. A creep model [39], which was developed based on the results of a group of creep tests, was used to obtain the creep deformation. Although the creep model was established by the curve fitting of the results from the standard triaxial tests, the model was verified to have the ability to describe the real creep effect of rockfill, particularly under high confining pressure [2,39]. Axial creep strain $\varepsilon_L(t)$ and time t were expressed by the power function as follows:

$$\varepsilon_L(t) = \varepsilon_{Lf}(1 - t^{-\lambda_L}), \tag{5}$$

where ε_{Lf} is the limit of axial creep strain, and λ_L is the coefficient related to the rate of axial creep strain. The values of ε_{Lf} and λ_L could be obtained from the correlation of axial creep and time for various test groups. The limit of axial creep ε_{Lf} was expressed as follows:

$$\varepsilon_{Lf} = \beta \cdot \sigma_3 = \frac{c_L \cdot S}{1 - d \cdot S}\sigma_3, \tag{6}$$

where σ_3 is the confining pressure, S is the stress level, c_L and d are the creep parameters that could be obtained from the fitting curve between β and S, coefficient β is the hyperbolic function of S, and λ_L is independent of S but is a power function of σ_3. Creep parameters η and m_L could be obtained from the fitting curve between λ_L and σ_3 as follows:

$$\lambda_L = \eta \cdot \sigma_3^{-m_L}. \tag{7}$$

Volume creep strain $\varepsilon_V(t)$ and time t were also expressed using the following power function:

$$\varepsilon_V(t) = \varepsilon_{Vf}(1 - t^{-\lambda_V}), \tag{8}$$

where ε_{Vf} is the limit of volume creep strain, and λ_V is the coefficient related to the volume creep strain rate. The limit of volume creep ε_{Vf} is expressed as follows:

$$\varepsilon_{Vf} = \alpha_V + \beta_V \cdot \sigma_3 = c_\alpha \cdot S^{d_\alpha} + c_\beta \cdot S^{d_\beta} \cdot \sigma_3, \tag{9}$$

where c_α, d_α, c_β and d_β are the volume creep parameters. λ_V is independent of S and σ_3 and was assumed as a constant.

The creep model had nine parameters, namely, c_L, d, η and m_L, which were defined for axial creep, and c_α, d_α, c_β, d_β and λ_V, which were defined for volume creep. These nine parameters could be obtained from a group of creep triaxial tests. Creep limit was nonlinear for both stress level and confining pressure. The complete details and the verification were indicated in [2,39].

During the modelling process, each calculation step produced both mechanical and creep responses. (a) The instantaneous strain was calculated under the current loading step. The stress and strain of each element were determined at the current load level end. (b) From the loading process, the duration time t of the current load was divided into numerous increments Δt. The stress and creep strain rate were assumed to remain unchanged during each period Δt, and the accumulative creep strain was assumed to be zero in the first calculation. The creep strain ratio could be computed for every short interval of Δt. The total creep could be obtained under the current load level. (c) After performing finite element method (FEM) analysis using the initial strain method, stress and strain increments could be obtained under the current load level, and the total stress and total strain could be determined until the end of the current loading step.

Table 4
Parameters of the elasto-plasticity model and the initial hydraulic conductivity.

Material	Density (g/cm^3)	K	m	φ_0 (°)	$\Delta\varphi$ (°)	R_f	G	F	D	k_0 (m/s)
Cushion	2.25	1400 (1448)	0.42 (0.44)	48	8.6	0.86	0.43(0.44)	0.30(0.32)	5.5	1.5×10^{-6}
Transition	2.23	1300 (1356)	0.42 (0.43)	49	8.7	0.87	0.41(0.42)	0.28(0.30)	5.2	2.1×10^{-4}
Main rockfill	2.35	1250 (1312)	0.45 (0.46)	53	8.5	0.89	0.37(0.39)	0.25(0.26)	5.2	3.2×10^{-3}
Sub rockfill	2.25	1050 (1149)	0.35 (0.36)	51	8.4	0.80	0.35(0.37)	0.26(0.30)	5.0	1.9×10^{-3}
Q_4^{a1}	2.20	1000 (1115)	0.43 (0.43)	43	8.6	0.78	0.30(0.32)	0.23(0.25)	4.6	1.7×10^{-4}
Q_4^{a2}	2.15	1200 (1427)	0.43 (0.41)	42	8.6	0.80	0.38(0.35)	0.26(0.25)	5.1	1.7×10^{-4}
Q_4^{a3}	2.20	1500 (1763)	0.42 (0.42)	42	8.5	0.81	0.42(0.45)	0.33(0.34)	5.3	1.4×10^{-4}

Note: Parameter values in parentheses were obtained via back analysis, whereas the remaining values were obtained via tests.

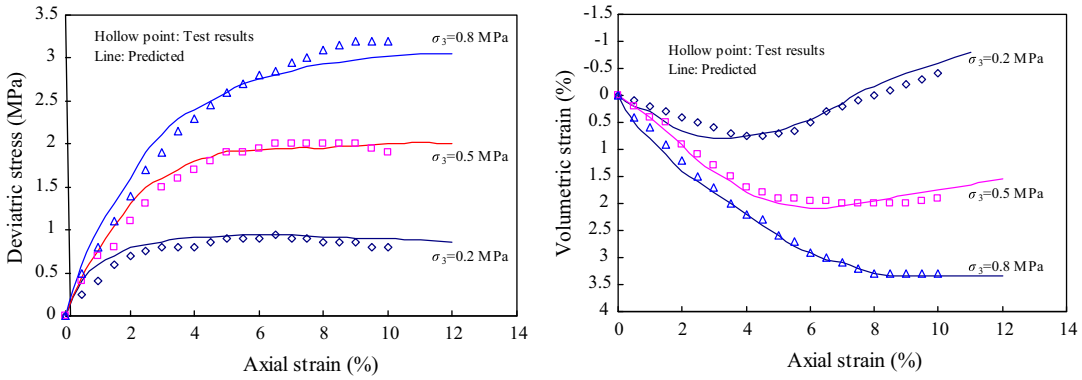

Fig. 8. Comparison of model predictions of stress–strain relationship of river gravels with triaxial test results.

The concrete and bedrock materials were simulated using a linear elastic model. The density, Poisson's ratio and hydraulic conductivity of the concrete material were 2.45 g/cm^3, 0.167 and 1.0×10^{-12} m/s, respectively. The elastic moduli for the face and toe slabs were both 28 GPa, whereas the elastic modulus for the cutoff wall was 26 GPa. The hydraulic conductivity for the cutoff wall and toe slab was 1.0×10^{-9} m/s. The density, elastic modulus, Poisson's ratio and hydraulic conductivity of the bedrock were 2.25 g/cm^3, 20 GPa, 0.231 and 2.0×10^{-7} m/s, respectively. Arici [42,43] stated that the rockfill–slab interface did not significantly affect the dam behaviour and cracking in the face slab based on the contact behaviour analysis of high CFRDs. In the present study, the Lagrange method based on contact mechanics in the Adina system [44] was used because of its simplicity. The contact tolerance was set to 0.5 mm, and the frictional coefficient was set to 0.22. The same method was used to simulate slab and peripheral joints.

4.3. Coupled HM analysis method

For a dam built on a foundation of low-permeability soil or soft clay, the consolidation caused by the long-term dissipation of the excess pore pressures of the foundation may continue at a significant rate over a long period. The river gravel foundation of the Miaojiaba CFRD was typical coarse granular materials with strong permeability. They were free draining, and the porosity was large. Different material structures, compared with soft clay, indicate that excess pore pressure dissipates rapidly without the typical consolidation effect. However, the deformation behaviour of CFRDs depends mainly on the mechanical and hydraulic properties of the construction materials. The HM coupling process can have a significant effect on the dam behaviour, especially when the dam is built on river gravel foundation below free surface after reservoir filling.

The coupled HM analysis method for CFRDs proposed in [32] was adopted in the current study. This method was successfully applied to the HM coupling analysis of Shuibuya Dam [32] and a deep alluvium foundation [16]. The deformation response of rockfill and river gravel was described using the adopted elasto-plasticity model. The capillarity effect through the coarse granular material, such as rockfills and river gravel, is generally negligible. The test results showed that the influence of water content on the strength of the rockfill and river gravel was less significant. Therefore, non-steady saturated seepage flow analysis was applied in this study. The variational inequality approach [32,45] with an adaptive penalised Heaviside function was adopted to determine the free surface and seepage points of the saturated flow process. The boundary conditions on the potential seepage surfaces were assumed as the complementary conditions of the Signorini's type. The coupled flow and stress process was governed by the momentum and mass conservation laws of continuum mechanics. In the framework of Biot's theory, the governing equations could be described as follows:

$$\begin{cases} \nabla \cdot [\mathbf{D} : \nabla(\frac{\partial u}{\partial t}) - \alpha \frac{\partial p_w}{\partial t}\delta] + \frac{\partial f}{\partial t} = 0 \\ [1 - H(\phi - z)]\rho_w(\frac{\partial \varepsilon_v}{\partial t} + S_w \frac{\partial \phi}{\partial t}) + \nabla \cdot (\rho_w v) = 0 \end{cases}, \tag{10}$$

where $\mathbf{D}$ is the tangential elastic modulus tensor, u is the displacement vector, α is Biot's coefficient, p_w is the pore water pressure, δ is the Kronecker delta tensor, f is the body force tensor, $H(\phi\text{-}z)$ is a Heaviside function, ρ_w is the density of water, ε_v is the volume strain, S_w is the specific storage towing to the compressibility of water, ϕ is the total water head and v is the flow velocity.

The dependence of permeability on stress is fundamental to understand the coupled processes. Changes in deformation and porosity result in permeability variations in rockfill and river gravel. In each construction step, the variation in permeability was updated with a modified Kozeny–Carman equation, which described the dependence of permeability on porosity and volumetric deformation. With the assumption of small deformation, the evolution of porosity was linked to volume strain.

$$\begin{cases} k = k_0\left(\frac{n}{n_0}\right)\left(\frac{1-n_0}{1-n}\right)^2 \\ n = 1 - (1 - n_0)\exp(\beta_1 \varepsilon_v) \end{cases}, \tag{11}$$

where k and k_0 are the current and initial hydraulic conductivities, respectively. n and n_0 are the current and initial porosities, respectively. $\beta_1 = 1$ if the grains were assumed to be non-deformable. The initial hydraulic conductivity (shown in Table 4) was obtained by field tests.

An interlaced algorithm was adopted to solve the HM processes until convergence criteria were satisfied. The mid-point incremental method was used to solve the nonlinear mechanical process. A parabolic variational inequality formulation of the Signorini's condition was used to determine the free surface and seepage points of the non-steady seepage process. The details of the HM analysis method could be found in [32,45]. At each time step, the coupled process was solved, and k was assumed to remain unchanged. The creep response was calculated, and k was updated for the next time step.

4.4. FE model

The 3D mesh used for numerical calculation is presented in Fig. 9. A total of 67,185 elements and 73,184 nodes were utilised. The model was simulated by using spatial eight-node isoparametric elements. Five rows of elements were divided in the thickness direction to reflect the behaviour of impervious structures accurately. The foundation was approximately divided into three layers

to consider the effectiveness of field compaction with depth and geological characteristics in the numerical simulation. The influence area of the field compaction was limited only to the Q_4^{a3} group river gravel, and thus Q_4^{a3} was simulated as the upper layer (compaction layer) of the foundation. Although field compaction of the foundation could improve density and bearing capacity to a certain extent, the effect of compaction on foundation behaviour was expected to be limited compared with the effect of the dam construction process. Therefore, the effectiveness of field compaction with depth was not considered further. The calculation parameters were obtained after compaction. The middle (Q_4^{a2}) and lower (Q_4^{a1}) layers of the foundation were divided according to the geological characteristics shown in Fig. 9.

The computational procedure followed the construction and subsequent reservoir-filling processes, as shown in Fig. 3. Before reservoir filling, the time step length was set according to the dam construction schedule. The construction of the face slab was simulated in three stages. Afterwards, the time step length was taken as 10 days, given the rising rate of the water level. The bottom boundary was fixed, and side boundaries were constrained in the normal direction. These boundaries were set as impermeable for the seepage analysis. On the upstream and downstream surfaces of the dam and the ground surface submerged in water, the water head was prescribed according to the fluctuation in the water level. The remaining boundaries were taken as the potential seepage boundaries, thereby satisfying Signorini's complementary condition. The initial water head distribution was determined with a steady-state seepage analysis before dam construction. The numerical modelling of the coupled HM process started on October 30, 2009 and ended on July 30, 2012.

4.5. Back analysis of model parameters

Obtaining reasonable mechanical parameters in laboratory tests is sometimes difficult because of the scale effect [39,46]. Back analysis, which is based on field-monitoring results, is a helpful technique for evaluating model parameters [2,34]. Back analysis was performed to obtain the model parameters for the method presented in [2]. This method combined hybrid genetic algorithms (HGAs) and FEM. The objective function was as follows:

$$f(x_1,x_2,\ldots,x_n)=\left\{\frac{1}{ks}\sum_{i=1}^{s}\sum_{j=1}^{k_1}[g_i(x_1,x_2,\ldots,x_n,t_j)-u_i(t_j)]^2\right\}^{0.5}, \tag{12}$$

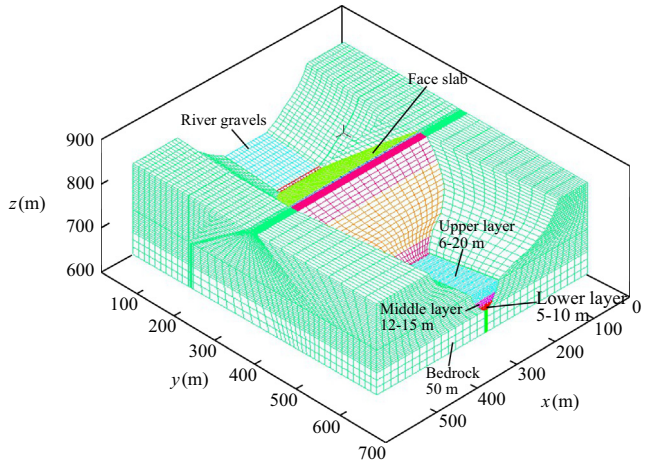

Fig. 9. 3D FE mesh of Miaojiaba CFRD.

where $x_1,x_2,\ldots,x_n$ is a group of parameters to be inverted, $g_i(x_1, x_2,\ldots,x_n, t_j)$ is the calculated deformation of the ith monitoring point at time t_j, $u_i(t_j)$ is the observed value, and s and k_1 are the numbers of monitoring and time points used in the back analysis, respectively.

On the basis of the HGA procedure, FE calculations were performed each time a fitness value was evaluated. The procedure for back analysis using HGA could be summarised as follows:

(1) An initial population $\mathbf{P}(j)=\{\mathbf{x}^1(j),\mathbf{x}^2(j),\ldots,\mathbf{x}^{p_1}(j)\}$ was generated, where j refers to the current generation, and p_1 is the individual number.
(2) The value of $g_i(x_1,x_2,\ldots,x_n, t_j)$ was obtained via FE simulation, and the objective function was calculated for each individual to evaluate $\mathbf{P}(j)$.
(3) Two individuals were randomly selected to perform crossover operation, and an offspring was generated. Mutation was then applied occasionally to maintain diversity.
(4) Three individuals with the smallest fitness were selected from the parent and offspring population. The approximate minimum point was evaluated. If the fitness of the approximate minimum point was smaller than that of the three selected individuals, then the individual with the largest fitness value in the offspring population would be replaced with the minimum point.
(5) After a knockout competition between each individual and its offspring, the winner was selected and promoted to the next generation.
(6) Steps 3–6 were repeated until the termination criteria were satisfied.

In back analysis, numerous parameters will require considerable monitoring point data and computational resources. The elasto-plasticity model had eight parameters, whereas the creep model had nine. Performing back analysis for all 17 parameters appeared impossible. Different parameters in the model had varying sensitivities to dam deformation [2,39,47]. The parameters c_L, η, c_α, c_β and λ_V of the creep model and K, m, G and F of the elasto-plasticity model were set as parameters for back analysis. The remaining parameters were obtained from laboratory tests. The observed settlements of 15 HSG monitoring points in cross section 0 + 194 were selected for the back analysis. The monitoring data covered the period from October 2009 to April 2012. The back analysis of creep model parameters was firstly performed according to the measured deformation after reservoir filling to reduce work load. The obtained creep model parameters were then set as constants, and back analysis of the elasto-plasticity model parameters was performed. Additional details of the back analysis method were presented in [2].

Before back analysis was performed, a group of laboratory tests were conducted to determine the model parameters. Thus, we were able to compare the back analysis parameter values with laboratory test values. The model parameter values of the elasto-plasticity and creep models obtained from the laboratory tests and the back analysis are presented in Tables 4 and 5, respectively. The simulated and observed settlements in cross section 0 + 194 for 8 months after reservoir filling are compared in Fig. 10. For comparison, the simulated settlements based on laboratory test parameters were also included. The values of K for the elasto-plasticity model obtained from the back analysis were larger than those obtained from the laboratory tests, and the values of m, G, and F were close. This finding might indicate that the deformation moduli of the rockfill under in situ compression conditions were larger than the laboratory test values. The values of c_L, η and c_β for the creep model obtained from back analysis were larger than

those obtained from laboratory tests, and the values of c_α and λ_V were smaller. However, all the parameter values were close without significant mutation. As shown in Fig. 10, the results based on laboratory test parameters were evidently larger than the measured values, but the results of the back analysis agreed well with the measured results. These results demonstrated that the current model and the back analysis parameters were reasonable.

5. Comparison of numerical results with in-situ measurements

5.1. Deformation of river gravel foundation

A comparison of settlement–time curves is given in Fig. 11 for settlement gauges VE2-4 and VE2-5, i.e. at the top of the foundation and 14 m below the surface, respectively (see Fig. 1b for the locations), to understand the deformation of the river gravel foundation and to obtain insights into the mechanisms that lead to high values of dam deformation. The measured settlements accumulated over time. During construction, settlement rapidly increased with a continuous increase in dam weight load. During reservoir filling, settlement increased with water pressure, but the deformation rate was slower than that during dam construction. The settlement increased mildly and tended to stabilise after reservoir filling. The trend was different for a dam constructed on a foundation of small permeability, which showed long-term deformation after reservoir filling because of the dissipation of excess pore water pressure. The measured maximum accumulated settlements at EoC and EoF were 707 mm and 800 mm at the top of the foundation, respectively.

As shown in Fig. 11, the larger dam deformations mainly resulted from three mechanisms. The first mechanism was the nonlinear compressive deformation (without considering creep and HM coupling) of the foundation caused by rock block sliding and rearrangement under dam weight and reservoir pressure. Although river gravel foundation had been compacted, 20% porosity remained, which provided a precondition to generate large compressive deformation. The compressive deformation accounted for 83.6% of the total deformation at EoF. The second mechanism was the foundation creep deformation caused by delayed grain fracture processes under a constant load. The creep deformation accumulated over time, but the deformation rate slowed down after reservoir filling. The maximum accumulative creep deformation was 60 mm at EoF, which accounted for 7.5% of the total deformation. The third mechanism was the deformation caused by the HM coupling process. The deformation caused by HM coupling mainly occurred during the reservoir-filling period. The maximum accumulative deformation caused by HM coupling process was 52 mm at EoF, which accounted for 6.5% of the total deformation. The numerical results considering creep and the HM coupling process still underestimated the settlements, especially during the impounding period, but the trend was similar to that of measured deformation. A possible reason for the underestimation with the maximum of 33 mm accounting for 4.1% of total settlement could be that the numerical model did not consider the wetting deformation and partly saturated soil behaviour. These analyses indicated that the foundation compressibility, creep and permeability governed the large dam deformation, in which foundation compressibility was the main factor that contributed to the large dam deformation, and creep and the HM coupling process were the main sources of the time-dependent deformation. The simulated settlements considering creep and HM coupling were also compared with the numerical results adopting E-B model. The predictions obtained using the E-B model were considerably smaller than those obtained using the elasto-plasticity model after construction. The maximum difference occurred during reservoir filling, with a value of 55 mm. The reason was related to the fact that plastic strain and dilatancy had a significant effect on the river gravel behaviour. These results provided evidence of the reasonable applicability of the elasto-plastic model in simulating the nonlinear behaviour of river gravel and rockfill.

Fig. 12 illustrates the evolutions of measured and simulated pore water pressures at two typical piezometers (P5, P6) installed in the foundation and another two typical piezometers (P1, P2) installed in the rockfill. The figure also shows the evolution of the leakage rate. During construction, the water table was very low; thus, no pore water pressure was observed. During reservoir filling, both the measured and simulated pressures increased and basically fluctuated with the reservoir level. At the end of reservoir filling, the pore water pressures approached the peak values, decreased mildly and tended to stabilise. Owing to the strong permeability, the excess pore pressure dissipated rapidly. The simulated water pressure agreed well with the measured one. The simulated results were generally larger than the measured results, especially for those of the foundation. However, the maximum difference was no more than 15 kPa during the entire stage. The evolutions of leakage rate were similar to the variations in pore water pressure. The maximum leakage rate was reached immediately after reservoir filling and decreased to a steady state in the long term.

Infiltration water would wet the rockfill below the free surface. Wetting could induce additional deformation (i.e. wetting deformation) mainly because of the reduction in the contact friction coefficient amongst particles and the crushing strength of a single particle [40,41]. Observational investigations in laboratory tests and field monitoring have indicated the possibility of wetting deformation of rockfill, as reported by several researchers [1,3,40,41,48]. However, only a significant portion of wetted rockfill could cause significant changes in rockfill deformation [3]. As shown in Fig. 12, seepage flow under the dam body was effectively prevented by the seepage control system given that the free surface was very low, the long-term leakage rate was as small as 30 l/s, and the pore water pressure under the dam body was less than 50 kPa. The sprinkling tests conducted during the compaction tests demonstrated that sprinkling water caused only an average dry density increase of 0.02 g/cm^3 for rockfill and 0.01 g/cm^3 for river gravel, which indicated that the rockfill and river gravel of the Miaojiaba CFRD were insensitive to the wetting effect. Therefore, the wetting deformation was expected to be limited in the Miaojiaba Dam, which was compacted without sprinkling water in the actual construction process, with an average water content of 2% after compaction.

Table 5
Parameters of the creep model.

Material	c_L	d	η	m_L	c_α	d_α	c_β	d_β	λ_V
Main rockfill	0.2507 (0.2745)	0.7968	0.0862 (0.1107)	0.3568	0.5437 (0.4879)	1.9872	0.3152 (0.3989)	1.4526	0.0721 (0.0606)
Sub rockfill	1.3624 (1.2153)	0.2247	0.1126 (0.1201)	0.9486	0.3462 (0.3027)	0.7254	0.2078 (0.2084)	0.9987	0.1044 (0.0899)
River gravels	1.4526 (1.3546)	0.2569	0.1937 (0.1457)	1.0253	0.3364 (0.3149)	0.5698	0.1564 (0.1779)	0.9156	0.1001 (0.0898)

Note: Parameter values in parentheses were obtained via back analysis, whereas the remaining values were obtained via tests.

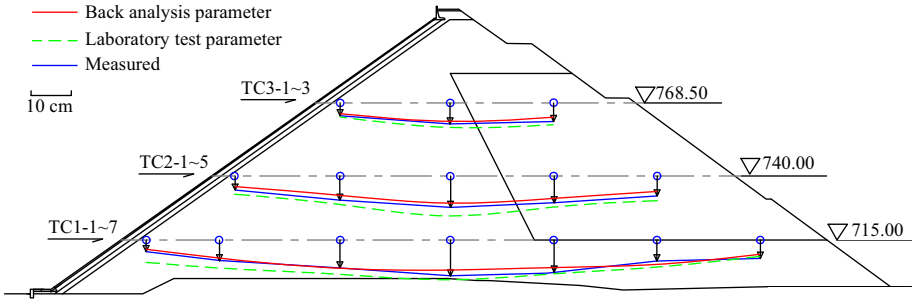

Fig. 10. Comparison between settlement results of measurement and numerical analysis in cross section 0 + 194 for 8 months after reservoir filling.

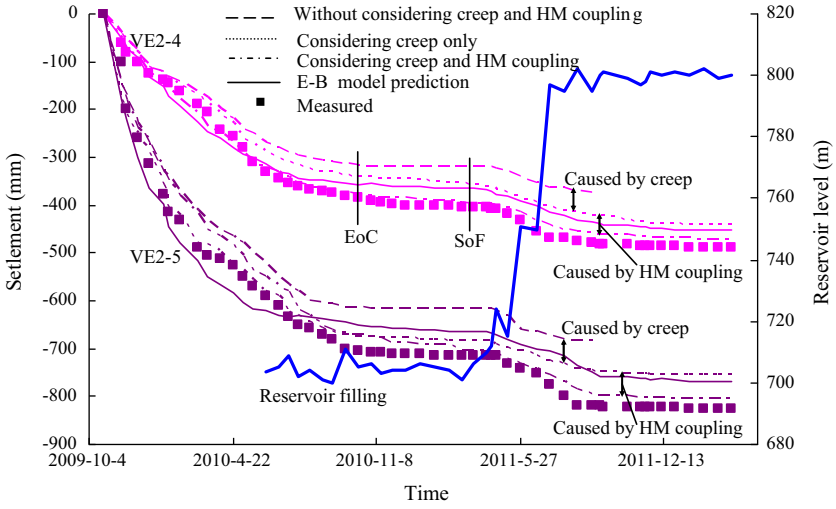

Fig. 11. Comparison of settlement–time curves for settlement gauges VE2-4 and VE2-5.

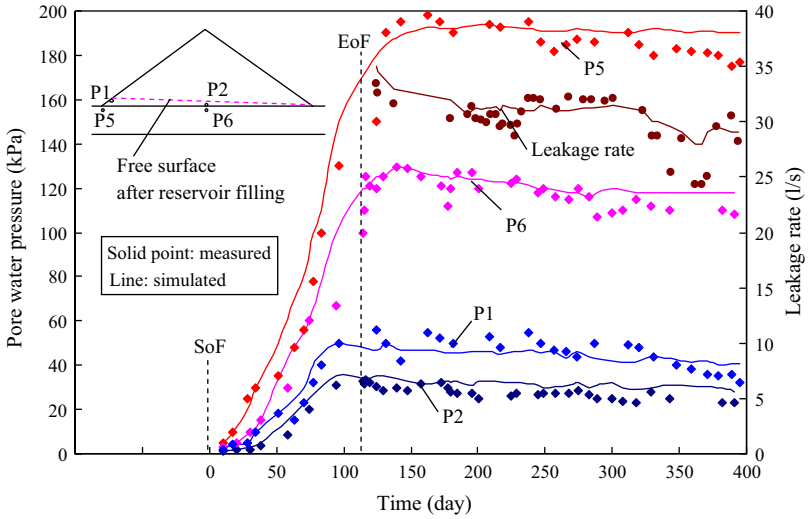

Fig. 12. Evolution of measured pore water pressure and leakage rate of Miaojiaba CFRD.

5.2. Deformation of dam body

Fig. 13 compares the accumulated settlement in cross section 0 + 194 at EoF and the incremental settlement and horizontal displacement caused by reservoir filling at the upstream slope. The measurement of the settlement contour was accomplished via linear interpolation of the measured values at the monitoring points. The simulated maximum accumulated settlements at EoC and EoF were 786 mm (0.71H%) and 882 mm (0.80H%) near the dam base (EL of 725 m), respectively, which were less than the measured values. The simulated settlements were in reasonable agreement with the measured values in the outside zones but were smaller than those in intermediate zones.

The first reservoir filling was a critical loading condition. For stiff-foundation dams, over half of the total settlements occurred during this stage [25]. The water load caused downstream

deformation, and maximum settlements occurred close to the centre of the upstream face and diminished towards the downstream face [29]. Fig. 13 shows that the measured maximum incremental settlement was 195 mm (0.18H%) at the upstream face near the dam base (EL of 725 m), and this value was larger than the simulated value. However, the distribution pattern was approximately the same. The simulated maximum incremental displacement caused by reservoir filling was 23.0 cm (0.21H%), which occurred near the dam base of the upstream face. The maximum incremental horizontal displacement and its location were nearly the same as those of the incremental settlement, which were related to dam height, foundation thickness and the lithology of the rockfill and foundation materials.

Fig. 14 shows the measured and simulated settlements of the three ESG monitoring lines by the end of dam construction and the incremental settlements caused by reservoir filling. Three points were immediately evident from the figure. Firstly, significant settlement deformation was observed in the foundation. Secondly, the settlements in the sub rockfill zone were larger than those in the main rockfill zone because of the weaker material in the former. Thirdly, maximum settlement occurred near the dam base. The incremental settlements caused by reservoir filling exhibited a B-shaped distribution in Fig. 14b, with a large increment at the upper and bottom parts of the dam and at the upper part of the foundation. This result was attributed to the large crest settlement and the foundation deformation.

As shown in Fig. 14, although only measured data of part of monitoring points were used to perform the back analysis, the settlements of the back analysis were in good agreement with the overall measured results. The simulated results using parameters from laboratory tests were larger than those of measured ones, although the trend was similar. The main reason might be that parameters from laboratory tests could not reflect the rockfill behaviour accurately. Compared with the simulated results using laboratory test parameters, the back analysis obtained more accurate results which were close to the measurements, indicating that the back analysis method was correct and effective, and the current model could describe the main behaviour of the dam.

The comparison of the settlements at three typical instruments, TC1-4, TC2-2 and TC3-3, is plotted in Fig. 15. The plots depict a similar trend of simulated (considering creep and the HM coupling process) and measured settlements. During the construction period, some differences between the simulated and measured results were noticeable. After construction, the differences tended to diminish, and the simulated settlements were considerably close to the measurements. The maximum relative difference approached 5.1% (42 mm) during construction, occurring in the intermediate zones close to the bottom. The deformation difference could be attributed to the limitations of the numerical model, including (1) difficulty in considering complex loading and ground conditions (e.g. rainfall infiltration, construction technique and heterogeneity of particle size distributions), (2) inadequate constitutive model (i.e. negligence of partly saturated soil behaviour, wetting deformation and material breakage) and (3) simplification of the geometric model (i.e. valley shape and geological characterisation). Amongst them, negligence of rainfall infiltration might be the main reason for the large discrepancies during the construction stage, whereas negligence of wetting deformation might be the main reasons for the maximum deviation that occurred in the intermediate zones. Although some discrepancies existed, the current model had provided reasonable estimates of the dam behaviour.

The dam settlements were affected by various factors. The simulated results under different conditions are also provided in Fig. 15 to analyse the relative contribution of various factors (i.e. compressibility, creep and HM coupling) on dam settlement. Firstly, the compressive deformation (instantaneous deformation without considering creep and HM coupling) was the main source of the dam deformation. The maximum accumulative nonlinear instantaneous deformation was 800 mm at EoF accounting for 90.3% of the total deformation. The simulated settlements were also compared with the numerical results adopting E-B model, which did not consider plastic deformation and dilatancy. The predictions obtained using the E-B model generally underestimated the dam settlement. The maximum difference occurred during reservoir filling, with a value of 40 mm accounting for 4.5% of the total deformation. These results provided evidence that plasticity and dilatancy affected the instantaneous behaviour of the dam. Secondly, creep response evidently influenced the behaviour of the Miaojiaba CFRD. The dam settlements when considering creep exhibited an evident increment compared with those without considering creep response. The maximum settlement of the dam at EoC when considering creep response was 40 mm more than that without considering creep response, which was an increase of 5.4%. The maximum settlement at EoF when considering creep response was 60 mm more than that without considering creep response, which was an increase of 7.3%. Similarly, rockfill creep might contribute approximately 13.8% or even higher to the final settlements of the Shuibuya Dam, with the highest CFRD (233 m) at present [39]. Hunter [49] indicated that for a well-compacted rockfill, a long-term crest settlement resulting from creep ranged from 0.05H% to 0.25H% for each log cycle of time. Creep response also led to stress relaxation to a certain extent and resulted in an increase in deformation and stress of the face slab. Thirdly, the HM coupling process caused incremental deformation. Chen et al. [32] concluded that the effect of seepage flow on the deformation of CFRDs built on stiff foundation was unremarkable based a

foundation thickness andthe lithology ofthe rockfill andfoundation materials.

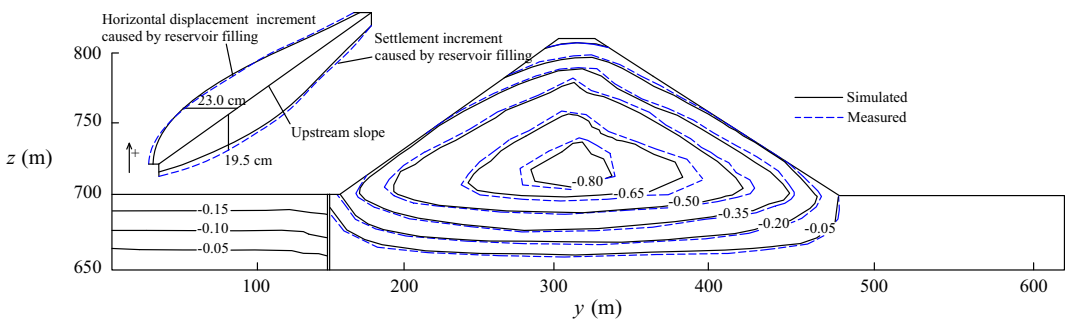

Fig. 13. Accumulated settlement in maximum cross-section at EoF (unit: m) and incremental settlement and horizontal displacement caused by reservoir filling at upstream slope.

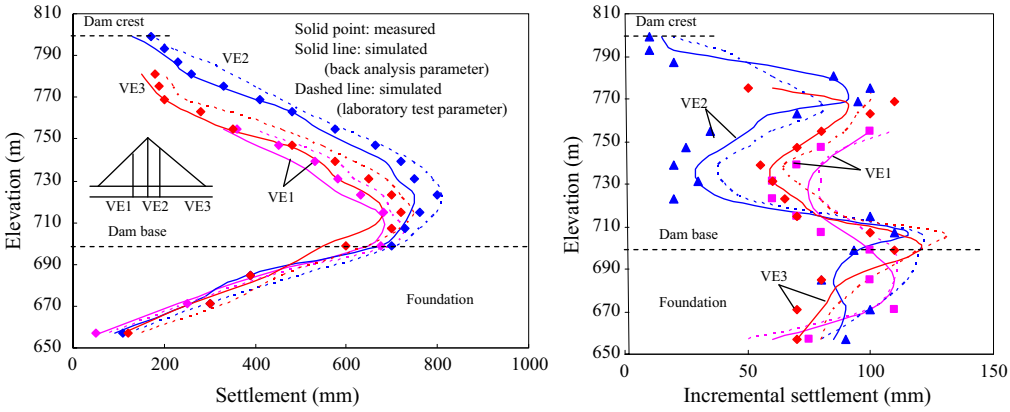

(a)Accumulated settlement at end of dam construction (b)Settlement caused by reservoir filling

Fig. 14. Internal settlement distributions at three ESG monitoring lines.

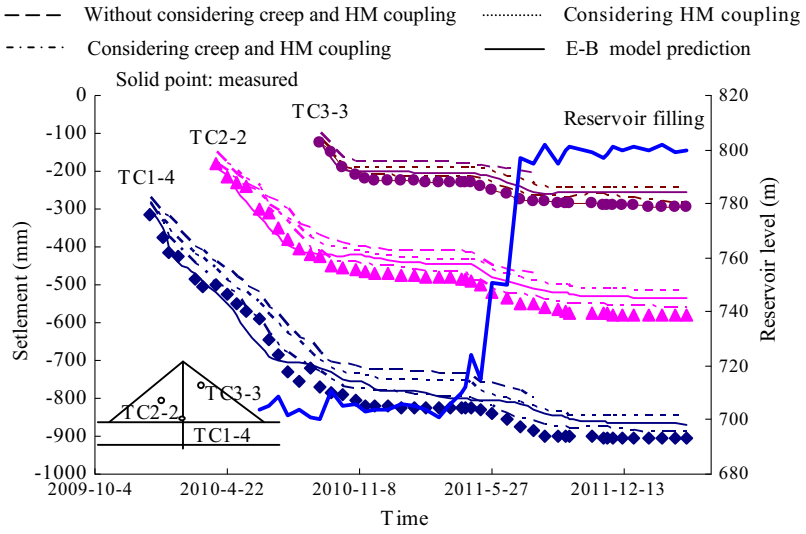

Fig. 15. Comparison of evolution of accumulated settlements at three typical settlement instruments.

coupled analysis. However, owing to the existence of river gravel foundation in the Miaojiaba Dam, the maximum settlement at EoF when considering HM coupling was 30 mm more than that without considering HM coupling, which accounted for 3.5% of the total deformation. Wetting deformation and partly saturated soil behaviour also could have a certain effect on the dam behaviour, but the effect was expected to be limited, as analysed previously. These analyses indicated that compressibility was the main factor that contributed to the dam deformation. Creep was responsible for the majority of long-term deformation of CFRDs on stiff foundation [2,4,39]. Nevertheless, the results showed that both creep and the HM coupling process had evident effects on the settlement of CFRDs on river gravel foundation, especially for the long-term settlement. The creep exhibited a relatively larger contribution of settlement to the dam body than the HM coupling process, considering that the HM coupling process mainly occurred in the foundation.

5.3. Stress of dam

The comparison of the vertical stresses at EoF is shown in Fig. 16. The maximum measured stress at EC2 was 1.81 MPa, whereas the simulated value was 1.65 MPa. The simulated and measured stresses and distributions were close to each other. These results confirmed that the numerical model was effective. The simulated major and minor principal stresses exhibited a distribution similar to vertical stress, with maximum values of 2.45 MPa and 1.41 MPa in the foundation bottom. Reservoir filling significantly changed the stress state only in the upstream face of the dam body and the foundation.

Valley shape was identified as a significant factor that affected the stresses within the dam because of the arching across abutment slopes [50]. Hunter and Fell [3] reported that when river width was approximately equal to half of the dam height and abutment slopes were steeper than 45°, vertical stress would be reduced by 10–20%. The river width of the Miaojiaba CFRD was 56 m (51H%), and the abutment slopes were approximately 47°. The bedrock and abutments considerably hindered further settlement deformation of the dam and the foundation. The arching effect was significant at the centreline of the maximum cross section, with the maximum reduction in vertical stress of 11%.

5.4. Behaviour of face slab

The deformations of impervious structures mainly depended on the deformation of the neighbouring dam bodies. Fig. 17 shows the

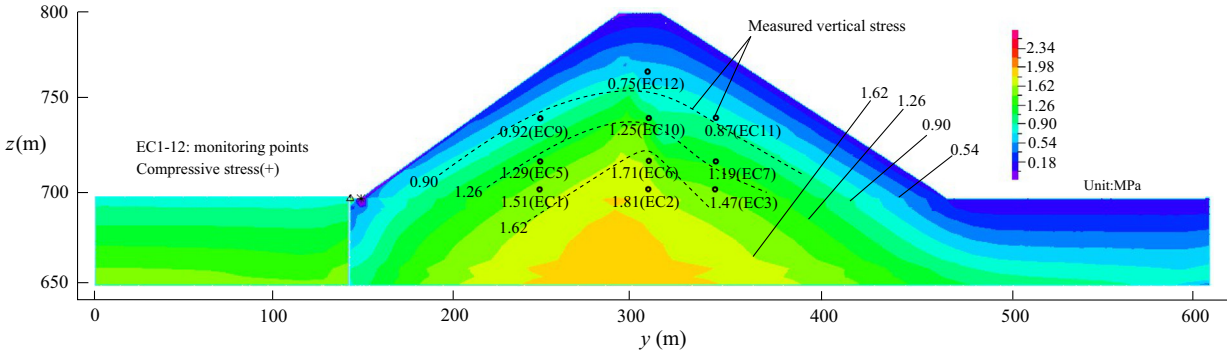

Fig. 16. Comparison of vertical stresses in cross section 0 + 199 at EoF.

simulated accumulative deformations of the seepage control system at EoF and the deformation of the face slab and the cutoff wall in a typical section. The maximum face slab deflection was measured at 5.2 cm (0.05H%) at EoC and 25.0 cm (0.23H%) at EoF, which occurred 28 m above the dam base (i.e. EL of 728 m). The deformation of the dam was the primary factor in face slab deformation. The simulated face slab deflections were similar to the determined values. Despite a few discrepancies, face slab deformation remained consistent with the D-shaped pattern of stiff-foundation dams [51]. The separation caused by the differential settlement between the face slab and the cushion layer could lead to cracks and seepage failure [33]. No separation was observed in the Miaojiaba CFRD.

Cracking, which is a key factor that affects dam safety, occurs when the tensile stresses induced in the face slab exceed the tensile strength [42,43]. The tension zone prior to reservoir filling was not developed, and the face slab was under compression because of its own weight, with a maximum compressive stress of 2.25 MPa, which occurred at the bottom. The simulated minor principal stress distribution at EoF is plotted in Fig. 18. The maximum major and minor principal stresses that occurred at the bottom were 6.54 MPa and 1.47 MPa, respectively. The face slab experienced tensile stresses in the downstream face near the toe, the crest and the abutments because of the moments caused by the large deflection and tension from the differential axial deformation and the settlement between the face slab and underlying rockfill. The measured slope direction stress of the face slab exhibited compressive behaviour in the middle, with a maximum stress of 8.4 MPa, and tensile behaviour in the abutments and bottom, with a maximum stress of 1.2 MPa. The measured horizontal direction stress exhibited a similar distribution to the slope direction stress. The stress distribution was consistent with the observations from stiff-foundation dams [20,33,34], thereby indicating that tension zones at EoF were mainly developed near the bottom and the abutments. Fig. 18 illustrates that the measured and simulated stresses and the tension zone were slightly different, which could be attributed to the previously described limitations of the numerical model. Overall, the measured maximum compressive and tensile stresses were within the acceptable range. No potential cracking and damage were developed in the face slab based on the simulated and measured tensile and compressive stresses.

5.5. Long-term deformation prediction

Additional FEA based on the numerical model was performed to predict the dam behaviour until December 2017 and to study post-construction deformation. The evolution of the predicted maximum crest and internal settlement and that of the maximum face slab deflection are shown in Fig. 19. Most of the deformation occurred before the completion of reservoir filling, and no significant long-term deformations were predicted. The reasons were likely twofold. Firstly, a few factors that could affect long-term

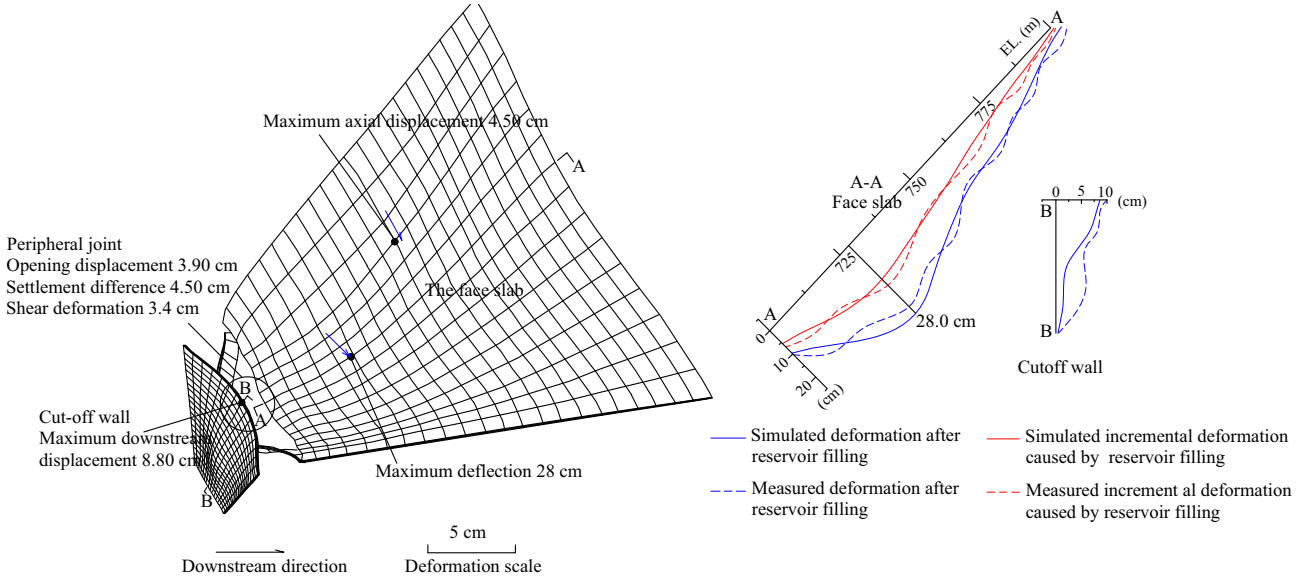

Fig. 17. Simulated accumulative deformations of impervious system at EoF and measured and simulated deformations of face slab and cutoff wall in a typical section.

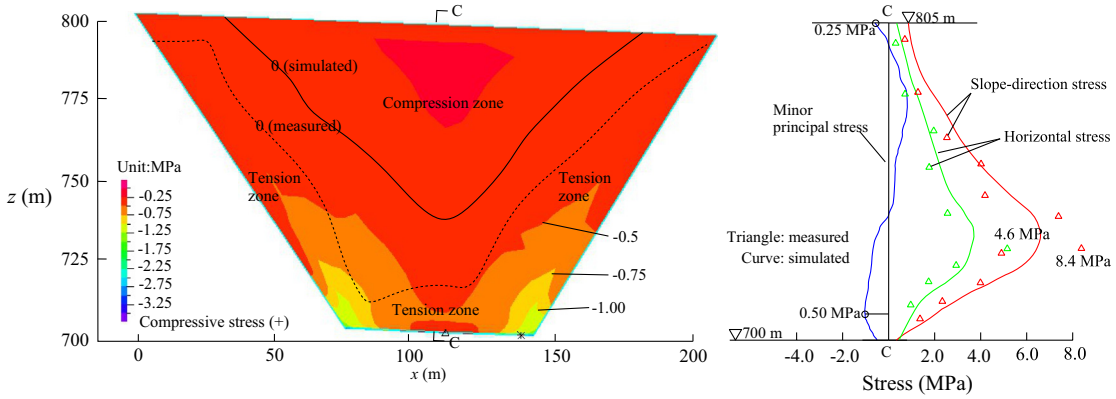

Fig. 18. Simulated minor principal stress distribution on downstream face of face slab at EoF and slope direction and horizontal stresses in a typical section.

settlements, such as wetting deformation, partly saturated soil behaviour and rainfall infiltration were not considered. However, the effects of these factors were expected to be limited and were difficult to consider [3,47,52]. Secondly, the nonlinear compressive deformation was the main cause of the dam deformation, which was generated during the construction and reservoir filling stages. In addition, most of the time-dependent deformation (creep and HM coupling) occurred before the completion of reservoir filling and slowed down after reservoir filling, thereby indicating that dam deformation tended to be stable. These deformations became stable after 2015. The increment in the internal settlement was less than 2 cm, and the settlement rate was expected to decrease to 0.83 mm per month from January 2016 to December 2017. The final accumulative internal settlement was approximately 0.94 m (0.85H%). The stable time for stiff-foundation dams was approximately 3–30 years after reservoir filling [20] (e.g. the Shuibuya Dam would become stable in approximately 4 years [2]). In this study, deformation slowed down in approximately 4 years, which was similar to the condition of Jiudianxia Dam which was also built on river gravel foundation [4]. The results indicated that the current dam deformation was basically stable. The predicted deformations using laboratory parameters were larger than those obtained by back analysis, but the trend laboratory parameters were similar to those of back analysis. The comparison confirmed that the back analysis method and the current model predicted correct results for the deformation process.

6. Behaviour of CFRDs built on river gravels

Monitoring results of 21 in-service CFRDs (no more than 150 m in height) built on river gravel foundation during the operation stage were collected for review to further understand the behaviour of CFRDs on river gravel foundation and to discuss their difference from stiff-foundation dams. Table 6 provides a comparison of the long-term deformations of the 21 CFRDs, including the Miaojiaba Dam.

Fig. 20 presents the maximum total internal settlement, face slab deflection and crest settlement measured at these CFRDs. For comparison, the summarised ranges of the corresponding deformations for stiff-foundation dams reported by other investigators are also plotted in the figure. The maximum internal settlements gradually increased with total height (including dam height and river gravel thickness). All of the internal settlements were less than 1.0H%. The magnitude of long-term face slab deflection appeared to be 0.1–0.4H%, but the Jiudianxia Dam exhibited a considerably larger value, which might result from large dam height (136 m) and river gravel thickness (50 m). The long-term crest settlement increased with total height, although the correlation was not clear. Nearly all of the crest settlements were less than 0.4H %. The deformation of the Miaojiaba Dam within the normal range appeared to be the same as that of the Chahanwushu Dam, which had similar dam height and river gravel thickness. The comparison indicated that the Mioajiaba Dam performed well, and the com-

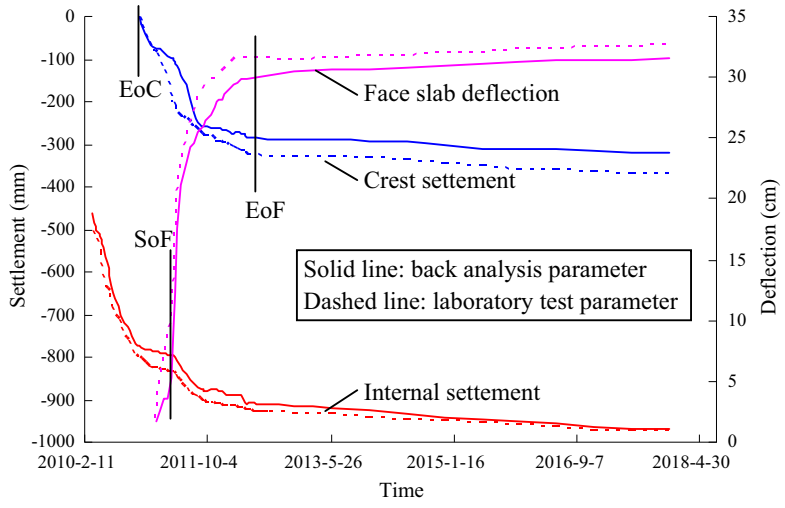

Fig. 19. Predicted time-dependent deformation of maximum settlement and deflection of face slab from construction stage to 5.5 years after reservoir filling.

Table 6
Dam details and deformation measurements for 21 in-service CFRDs built on river gravel foundation.

Name	Country	Year	Height (m)	Foundation and thickness	Rockfill	Surveyed period (year)	Crest settlement		Face deflection		Internal settlement	
							(m)	(H%)	(m)	(H%)	(m)	(H%)
Pappadai	Italy	1992	27	Gravel, 50 m	Calcarenite	7	0.01	0.04	–	–	0.07	0.26
Namgang	Korea	1999	34	Rock, gravel	Gneiss	5	0.01	0.04	0.06	0.17	0.11	0.32
Meixi	China	1998	41	Gravel, 30 m	Tuff	10	0.08	0.20	0.13	0.32	0.20	0.48
Kekeya	China	1981	42	Sand gravel, 37.5 m	Gravels	7	0.03	0.07	–	–	–	–
Dahe	China	1998	50.8	Sand gravel, 37 m	Sandstone	8	0.12	0.23	–	–	0.25	0.49
Shuangxikou	China	2009	52.1	Gravel, 15.4 m	Tuff	2	–	–	0.17	0.32	0.46	0.94
Pichi Leufu	Argentina	1999	54	Sand gravel, 28 m	Gravels	8	0.13	0.24	0.16	0.30	0.50	0.90
Kangaroo creek	Australia	1969	60	Rock, gravel	Schist	20	0.12	0.19	–	–	–	–
Mackintosh	Australia	1981	75	Weathered rock	Greywacke	20	0.24	0.32	0.25	0.33	0.48	0.64
Puclaro	Chile	1999	83	Sand gravel, 113 m	Gravels	5	0.11	0.13	0.12	0.14	0.67	0.81
Laodukou	China	2009	96.6	Sand gravel, 29.6 m	Gravels	2	–	–	0.11	0.11	0.34	0.35
Nalan	China	2005	109	Gravel, 24.3 m	Sandstone	6	0.16	0.15	0.16	0.15	0.31	0.28
Chahanwushu	China	2009	110	Sand gravel, 46.7 m	Sandstone	2	0.22	0.20	0.30	0.27	0.53	0.48
Miaojiaba	China	2011	110	Sand gravel, 50 m	Tuff	1	0.28	0.26	0.30	0.27	0.91	0.83
Duonuo	China	2012	112.5	Gravel, 35 m	Sandstone	2	0.33	0.30	0.23	0.20	1.10	0.98
Santa Juana	Chile	1995	113.4	Gravel, 30 m	Gravels	4	0.01	0.01	–	–	–	–
Reece	Australia	1986	122	Gravel	Dolerite	15	0.22	0.18	0.26	0.21	0.23	0.19
Shanxi	China	2000	132.5	Sand gravel, 24 m	Tuff	6	–	–	0.20	0.15	0.95	0.72
Jiudiaxia	China	2008	136	Gravel pebble, 50 m	Limestone	3	0.42	0.31	0.84	0.62	1.24	0.91
Alto anchicaya	Columbia	1974	140	Gravel	Hornfels	10	0.15	0.11	0.16	0.11	0.63	0.45
Xingo	Brazil	1993	140	Gravel	Granite	6	0.53	0.35	0.51	0.34	2.9	1.93

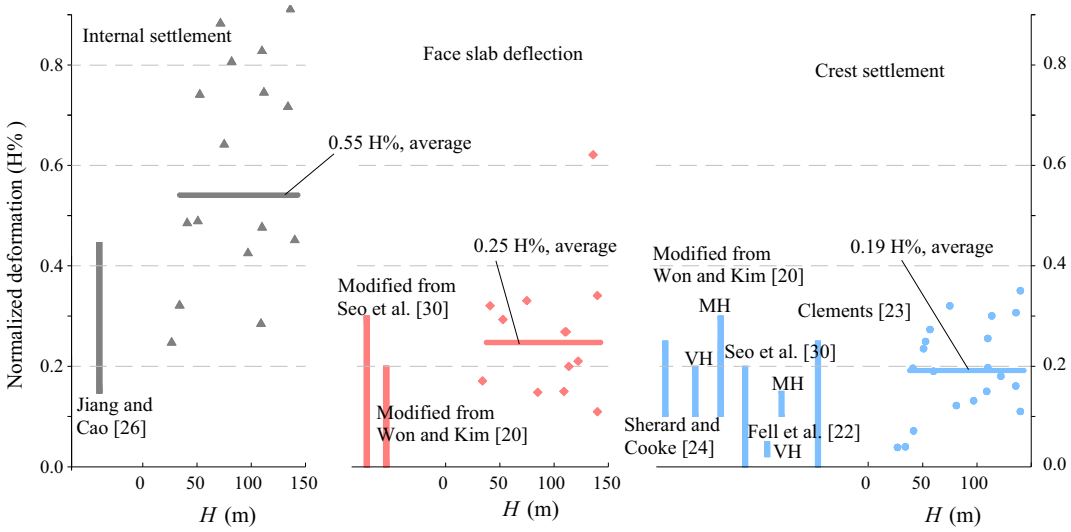

Fig. 20. Maximum total internal settlement, face slab deflection and crest settlement of 12 CFRDs built on river gravel foundation with respect to dam height.

paction effort used to control the foundation deformation was effective.

Most of the normalised internal settlements were larger than the range of the stiff-foundation dams. The ranges of the face slab deflection and crest settlement of the dams built on river gravels were considerably larger than the ranges of stiff-foundation dams, which could be both summarised as 0–0.3H%. Most of the dams listed in Table 6 showed that the internal settlement was maximised at the range of 0.2–0.4H from the dam bottom. The location of the maximum settlement moved downward with increases in the proportion of foundation thickness and dam height. The location was lower than the location of stiff-foundation dams, with the range of 0.4–0.6H [25]. Compared with stiff-foundation dams, both the crest settlement and face slab deflection could have an increase of 0.1%H, and the location of the maximum deformations could move down to 0.2H under the effect of foundation deformation.

The behaviour of CFRDs built on river gravel foundation was affected by many factors, such as the deformation characteristics of river gravel and bedrock topography. The effect of river gravel foundation would be significant when the foundation has large deformation modulus or the bedrock topography is wide. In Fig. 20, we considered dam height but disregarded other influencing factors, which resulted in discrete and irregular data points, but the results still provided useful insights into the behaviour of CFRDs on river gravel foundation.

7. Conclusions

In-situ measurements and numerical predictions of the behaviour of a CFRD built on river gravel foundation were presented. Comparisons were made between the predictions and the in-situ measurements in terms of deformations. The measured and numerical results were also compared with the case histories of stiff-foundation dams to examine the behaviour differences. The behaviour of a CFRD built on river gravel foundation was analysed comprehensively. The effect of the river gravel foundation on the

dam behaviour was discussed. The deformation mechanisms of the river gravel and the relative contribution of various factors on the CFRD behaviour were analysed quantitatively through numerical analysis. The following conclusions could be drawn from the results:

(1) Owing to the effect of foundation deformation, the deformations of the Miaojiaba Dam exhibited an evident increment compared with those of stiff-foundation dams, but they were still reasonable. The measured and predicted dam deformations indicated that the Miaojiaba Dam performed well, and the dam deformation was basically stable. In-situ measurements confirmed that the compaction effort used to control foundation deformation was effective, and river gravels could be used as CFRD foundation. For the CFRDs (no more than 150 m in depth) built on river gravel foundation, both the crest settlement and face slab deflection could have an increase of 0.1%H, and the location of the maximum deformations could move down to 0.2H compared with the stiff-foundation dams. This study provided important references for the design and assessment of CFRDs built on river gravel foundation.
(2) The foundation compressibility, creep and HM coupling process were the main mechanisms that resulted in large dam deformation, in which foundation compressibility was the main factor contributing to the foundation deformation, and creep and HM coupling process were the main sources of time-dependent deformation. Compressive deformation of the rockfill was the main factor that contributed to the dam deformation, and creep exhibited a relatively larger contribution of deformation to the dam body than the HM coupling process.
(3) The numerical results were in good agreement with in-situ measurements, demonstrating that the current model could capture the main behaviour of the dam, and the back analysis method was accurate and effective. The numerical model was reasonably effective for predicting the behaviour of an established dam with reliable monitoring data.

Acknowledgements

This study was supported by programme 2013KCT-15 of the Shanxi Provincial Key Innovative Research Team and the National Natural Science Foundation of China (51409206, 51409208 and 51579207). The authors are grateful to Sinohydro Corporation Engineering Bureau 15 CO., LTD for providing in-situ observation data.

References

[1] Xing H-F, Gong X-N, Zhou X-G, Fu H-F. Construction of concrete-faced rockfill dams with weak rocks. J Geotech Geoenviron Eng 2006;132(6):778–85.
[2] Zhou W, Hua J, Chang X, Zhou C. Settlement analysis of the Shuibuya concrete-face rockfill dam. Comput Geotech 2011;38(2):269–80.
[3] Hunter G, Fell R. Rockfill modulus and settlement of concrete face rockfill dams. J Geotech Geoenviron Eng 2003;129(10):909–17.
[4] Gan L, Shen Z-Z, Xu L-Q. Long-term deformation analysis of the Jiudianxia concrete-faced rockfill dam. Arab J Sci Eng 2013;39(3):1589–98.
[5] Ito M, Azam S. Engineering properties of a vertisolic expansive soil deposit. Eng Geol 2013;152(1):10–6.
[6] Wang YS, Liu SH. Treatment for a fully weathered rock dam foundation. Eng Geol 2005;77(1–2):115–26.
[7] Chai J, Igaya Y, Hino T, Carter J. Finite element simulation of an embankment on soft clay-case study. Comput Geotech 2013;48:117–26.
[8] Lollino P, Cotecchia F, Lidija Zdravkovic, Potts DM. Numerical analysis and monitoring of Pappadai dam. Can Geotech J 2005;42:1631–43.
[9] Karim MR, Gnanendran CT, Lo SR, Mak J. Predicting the long-term performance of a wide embankment on soft soil using an elastic-viscoplastic model. Can Geotech J 2010;47:244–57.
[10] Ozcoban S, Berilgen MM, Kilic H, Edil TB, Ozaydin IK. Staged construction and settlement of a dam founded on soft clay. J Geotech Geoenviron Eng 2007;133(8):1003–16.
[11] Oliveira PJV, Lemos LJL, Coelho PALF. Behavior of an atypical embankment on soft soil: field observations and numerical simulation. J Geotech Geoenviron Eng 2010;136(1):35–47.
[12] Lo SR, Mak J, Gnanendran CT, Zhang R, Manivannan G. Long-term performance of a wide embankment on soft clay improved with prefabricated vertical drains. Can Geotech J 2008;45:1073–91.
[13] Haan ED, Feddema A. Deformation and strength of embankments on soft Dutch soil. Proc ICE – Geotech Eng 2013;166(3):239–52.
[14] Kovacevic N, Higgins KG, Potts DM, Vaughan PR. Undrained behaviour of brecciated upper lias clay at Empingham Dam. Geotechnique 2007;57(2):181–95.
[15] Karstunen M, Yin ZY. Modelling time-dependent behaviour of Murro test embankment. Geotechnique 2010;60(10):735–49.
[16] Wang M, Chen YF, Hu R, Liu W, Zhou CB. Coupled hydro-mechanical analysis of a dam foundation with thick fluvial deposits: a case study of the Danba Hydropower Project, Southwestern China. Euro J Environ Civil Eng 2016;20(1):19–44.
[17] Wang W, Hoeg K, Zhang Y. Design and performance of the Yele asphalt-core rockfill dam. Can Geotech J 2010;47:1365–81.
[18] Xu Z, Hou YJ, Liang J, Han L. Centrifuge modelling of concrete faced rockfill dam built on alluvium. In: Proc 6th int conf on physical modeling in geotechnics. London: Taylor & Francis Group; 2006. p. 435–40.
[19] Wen L, Qin Y, Chai J, Li Y, Wang X, Xu Z. Behaviour of concrete-face rockfill dam on sand and gravel foundation. Proc ICE – Geotech Eng 2015;168(5):439–56.
[20] Won MS, Kim YS. A case study on the post-construction deformation of concrete face rockfill dams. Can Geotech J 2008;45(6):845–52.
[21] Lawton FL, Lester MD. Settlement of rockfill dams. In: Proc the 8th ICOLD congress ICOLD, Edinburgh, Scotland. p. 599–613.
[22] Fell R, MacGregor P, Stapledon D, Bell G. Geotechnical engineering of dams. Rotterdam, The Netherlands: Balkema; 2005.
[23] Clements RP. Post-construction deformation of rockfill dams. J Geotech Eng 1984;110(7):821–40.
[24] Sherard JL, Cooke JB. Concrete-face rockfill dam: I. Assessment. J Geotech Eng 1987;113(10):1096–112.
[25] Kim YS, Seo MW, Lee CW, Kang GC. Deformation characteristics during construction and after impoundment of the CFRD-type Daegok Dam, Korea. Eng Geol 2014;178:1–14.
[26] Jiang G, Cao K. Concrete face rockfill dams in China. Proceedings of the international symposium on high earth-rockfill dams, Beijing, vol. 3. p. 25–37.
[27] Xu B, Zou D, Liu H. Three-dimensional simulation of the construction process of the Zipingpu concrete face rockfill dam based on a generalized plasticity model. Comput Geotech 2012;43:143–54.
[28] Fitzpatrick MD, Cole BA, Kinstler FL, Knoop BP. Design of concrete-faced rockfill fam. In: Proc sym on concrete face rockfill dams: design, construction and performance. New York: ASCE; 1985. p. 410–34.
[29] Özkuzukiran S, Özkan MY, Özyazicioğlu M, Yildiz GS. Settlement behaviour of a concrete faced rock-fill dam. Geotech Geol Eng 2006;24(6):1665–78.
[30] Seo MW, Ha IS, Kim YS, Olson SM. Behavior of concrete-faced rockfill dams during initial impoundment. J Geotech Geoenviron Eng 2009;135(8):1070–81.
[31] Mahabad NM, Imam R, Javanmardi Y, Jalali H. Three-dimensional analysis of a concrete-face rockfill dam. Proc ICE – Geotech Eng 2014;167(4):323–43.
[32] Chen Y, Hu R, Lu W, Li D, Zhou C. Modeling coupled processes of non-steady seepage flow and non-linear deformation for a concrete-faced rockfill dam. Comput Struct 2011;89(13–14):1333–51.
[33] Zhang B, Wang JG, Shi R. Time-dependent deformation in high concrete-faced rockfill dam and separation between concrete face slab and cushion layer. Comput Geotech 2004;31(7):559–73.
[34] Wang Z, Liu S, Vallejo L, Wang L. Numerical analysis of the causes of face slab cracks in Gongboxia rockfill dam. Eng Geol 2014;181:224–32.
[35] Zhang G, Zhang JM, Yu Y. Modeling of gravelly soil with multiple lithologic components and its application. Soil Found 2007;47(4):799–810.
[36] Xiao Y, Liu H, Chen Y, Jiang J, Zhang W. State-dependent constitutive model for rockfill materials. Int J Geotech 2015;15(5):04014075.
[37] Zhang G, Zhang JM. Numerical modeling of soil–structure interface of a concrete-faced rockfill dam. Comput Geotech 2009;36(5):762–72.
[38] Zhang G, Zhang JM. Modeling of low-cement extruded curb of concrete-faced rockfill dam. Can Geotech J 2011;48(1):89–97.
[39] Zhou W, Chang X, Zhou C, Liu X. Creep analysis of high concrete-faced rockfill dam. Int J Numer Meth Biomed Eng 2010;26(11):1477–92.
[40] Zhao Z, Song E. Particle mechanics modeling of creep behavior of rockfill materials under dry and wet conditions. Comput Geotech 2015;68:137–46.
[41] Silvani C, Desoyer T, Bonelli S. Discrete modelling of time-dependent rockfill behaviour. Int J Numer Anal Meth Geomech 2009;33:665–85.
[42] Arici Y. Investigation of the cracking of CFRD face plates. Comput Geotech 2011;38(7):905–16.
[43] Arici Y. Behaviour of the reinforced concrete face slabs of concrete faced rockfill dams during impounding. Struct Infrastruct Eng 2013;9(9):877–90.
[44] Bathe KJ. Adina theory and modeling guide. Adina, vol. Volume I. Watertoen (WA, USA): Adina R&D Inc; 2003. p. 399–417.
[45] Chen Y, Hu R, Zhou CB, Li D. A new parabolic variational inequality formulation of Signorini's condition for nonsteady seepage problems with complex seepage control systems. Int J Numer Anal Meth Geomech 2011;35:1034–58.

[46] Gurbuz A. A new approximation in determination of vertical displacement behavior of a concrete-faced rockfill dam. Environ Earth Sci 2011;64 (3):883–92.
[47] Wei K, Zhu S. Application of an elastoplastic model to predict behaviors of concrete-faced rock-fill dam under complex loading conditions. J Civil Eng Manage 2015;21(7):854–65.
[48] Mahinroosta R, Alizadeh A, Gatmiri B. Simulation of collapse settlement of first filling in a high rockfill dam. Eng Geol 2015;187:32–44.
[49] Hunter GT. The pre- and post-failure deformation behavior of soil slopes Ph.D. thesis. Sydney (Australia): University of New South Wales; 2003.
[50] Giudici S, Herweynen R, Quinlan P. HEC experience in concrete faced rockfill dams-past, present and future. In: Proc int sym on concrete face rockfill dams, international commission on large dams, Paris. p. 29–46.
[51] Li Z. Defirmation observation on Longxi concrete face rockfill dam. Proc int sym on high earth-rockfill dams, Beijing, vol. 2. p. 514–21.
[52] Dounias GT, Kountouris A, Anastasopoulos K. Long-term behaviour of embankment dams: seven Greek dams. Proc ICE – Geotech Eng 2012;165 (3):157–77.